dynardo

dynamic software & engineering

ISSUE 2/2019

RDO-JOURNAL

optiSLang

SoS

ARTIFICIAL INTELLIGENCE AND MACHINE LEARNING APPLIED IN COMPUTER AIDED ENGINEERING

Every industry has high expectations in AI as a promising technology to promote current and create new business opportunities. Over the last decade, AI-based research has developed different powerful mathematical tools to mimic natural intelligence with the help of computers.

The AI-based metamodeling functionality is especially important for digital twins or autonomous drive applications. Here, the understanding of the response variability of a large data set and its correlation to input variability has to be considered.

For example, since more and more vehicles have been equipped with Advanced Driver Assistance Systems (ADAS), researchers and industries pay constantly growing attention to such technologies. One of the most important aspects for releasing ADAS is testing and validation. The mileage needed to proof the probability of system failure is impossible to reach in field operational tests. Therefore, statistical methods combined with Software-in-the-Loop (SiL) simulation have to be used. Beside meta-modeling, the field of reliability analysis provides algorithms and approaches which can be applied to assess ADAS by simulation. Due to the different kind of parameters and criteria, available methodologies need to be analyzed and adapted to ADAS specific challenges. By using predefined distribution functions for each input parameter, metamodeling combined with reliability analysis obtains safety statements with the approximation of the probability of failure for each traffic scenario. Here, multiple steps of different algorithms are combined to ensure trustworthy results and efficient procedures to be able to manage the necessary number of simulation runs.

The title story of this magazine wants to clarify what is "new" in the context of AI for CAE, especially regarding Machine Learning (ML) algorithms. The availability of large data sets combined with rising computation power creates a high potential for using ML in meta-modeling. Classical regression methods and AI-based algorithms for metamodeling are compared and discussed regarding the problem of overfitting, reachable forecast quality and related numerical effort to generate the meta-models. Furthermore, the initialization of machine learning algorithms and the integration of this technology into Dynardo's software tools is discussed and a first implementation of deep learning neural networks using Google's TensorFlow Library is introduced.

Apart from that, we again have selected case studies and customer stories concerning CAE-based Robust Design Optimization (RDO) applied in different industries.

I hope you will enjoy reading our magazine.

Yours sincerely

Johannes Will
Managing Director DYNARDO GmbH

Weimar, May 2019

CONTENT

ARTIFICIAL INTELLIGENCE AND MACHINE LEARNING APPLIED IN COMPUTER AIDED ENGINEERING

Self-learning algorithms prove high potential in metamodeling for CAE-based applications. Especially if large amounts of data from simulation or experiments are available, they outperform "classic" regression methods.

Introduction

Artificial Intelligence (AI) is the new shooting star in science and every industry has high hopes in using the "new" technology for almost everything. In this article, we would like to discuss what is "new" in AI for Computer Added Engineering (CAE) and what we can expect using AI-based technology for CAE applications. Starting with Wikipedia (en.wikipedia.org/wiki/Artificial_intelligence): "In computer science, artificial intelligence (AI), sometimes called machine intelligence, is intelligence demonstrated by machines, in contrast to the natural intelligence displayed by humans and animals. Colloquially, the term "artificial intelligence" is used to describe machines that mimic "cognitive" functions that humans associate with other human minds, such as "learning" and "problem solving". Continuing in related articles, we can extract that, like AI, different mathematical tools, which mimic natural intelligence by machine intelligence using computers, are understood. By searching for CAE applications, we will find several methods which are well known for a long time. This is mainly the methodology for solving optimization problems inspired by nature, such as evolutionary algorithms including genetic programming, swarm intelligence, as well as simulated annealing or, inspired by the human brain, so-called Artificial Neural Networks (ANN) are used.

Especially so-called Machine Learning (ML) algorithms extending ANN to deep forward neural or deep recurrent network as well as using support vector machines, which have made significant progress in the last decades, is indeed "new" in the context of AI for CAE. Taking advantage of that new technology and the availability of large data set and rising compute power, we expect that ML has a large potential for surrogate modeling. In purely mathematically driven surrogate models, often called meta-models, the learning process tries to understand how the response variability of a data set is correlated to variability of the inputs directly on the available data sets without further assumptions on the underlying physics. The required data may be collected from real measurements as applied for digital twins or in autonomous drive applications or may be obtained from simulations typically used in CAE based design.

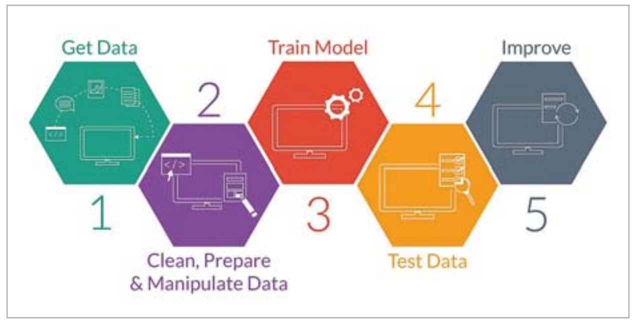

Fig. 1: Typical steps of machine learning algorithms (Source: www.machine-learning-blog.com)

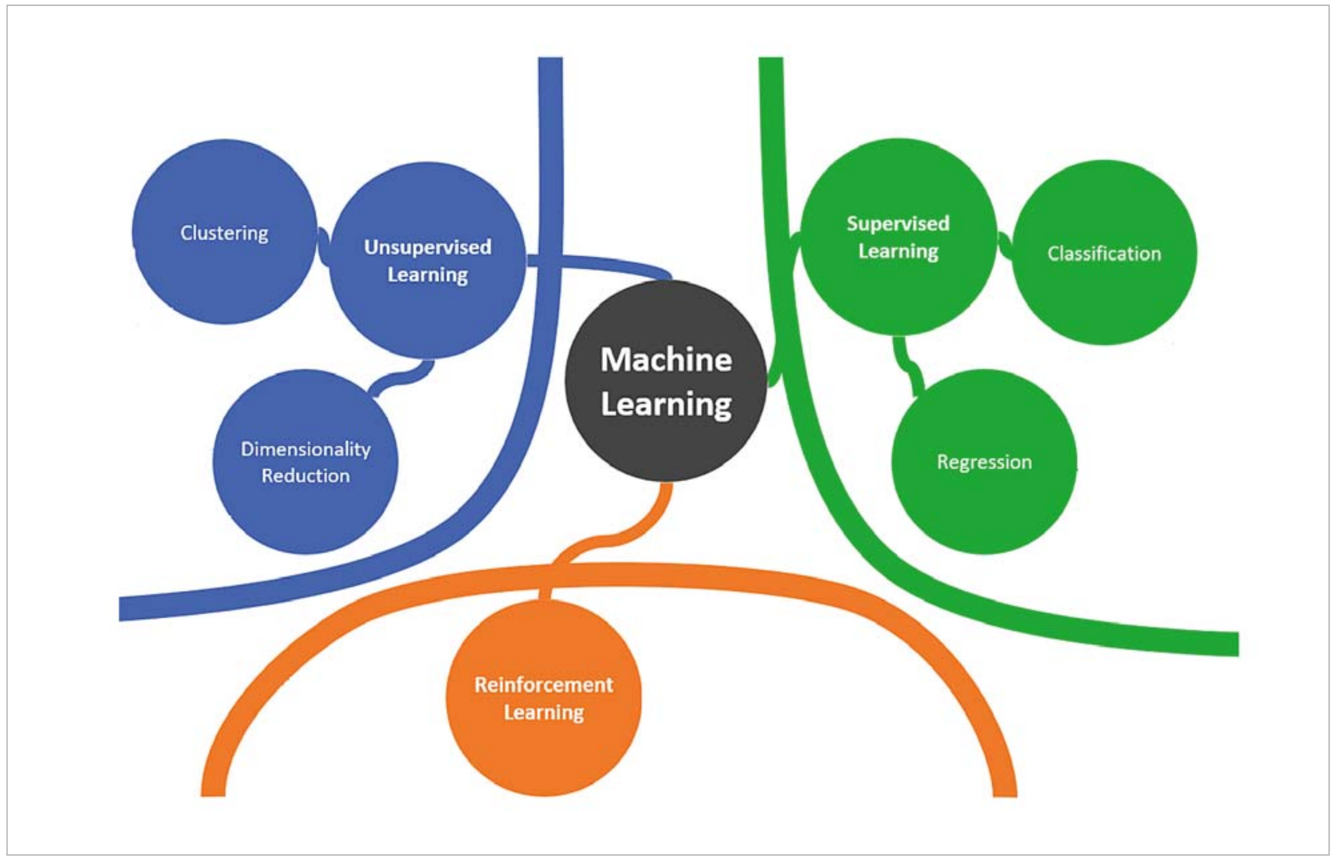

Fig. 2: Overview on different Machine Learning strategies (Source: www.morethandigital.info)

Of course, using correlation and regression analysis for meta-modeling, the process of clean, train, test data and try to learn what is the best combination of dimensionality and basis function is also not really new. Therefore, this article will start with introducing classical regression methods for meta-modeling, discussing the problem of overfitting, which does not disappear with machine learning, define machine learning algorithms and finally present the integration of machine learning technology into Dynardo's software tools.

Classical regression methods

In classical regression methods, a defined set of basis functions is used to set up a mathematical response surface model. Linear regression (Montgomery 2003) with linear or higher basis functions are a common basic approach, where a global set of basis functions is defined for a specific problem and for each basis function term the corresponding coefficient has to be calculated. Often this is done by a minimized least squares approach, in which the squared errors between data and model approximation are minimized. If the chosen global basis terms are not suitable to represent a physical phenomenon, this obtained response surface function is even in cases with sufficient high number of data points often not acceptable accurate.
In contrast to the global approach, local response surface methods like Moving Least Squares, Radial Basis Functions, or Kriging use basis terms with local support functions. With the help of a scaling factor the area of this local support can be defined. All available data points are usually considered as support of these local basis functions. This means, with increasing the data amount, the approximation quality of these local models raises. But in case of noisy data points, caused by solver noise in CAE or measurement errors in experimental analyses, such local models may tend to overfitting, by representing artificial oscillations in the approximation function. The overfitting needs special attention in the training and in the quantification of the accuracy of the surrogate model.

In the classical response surface approach, usually a specific model type and basis terms are chosen and trained with the data and later the approximation quality is quantified by some error measure. Often the Coefficient of Determination (CoD) as a measure of the goodness of fit is used for this purpose. Unfortunately, measuring the accuracy of fit is only suitable in cases, when the underlying regression model is not arbitrary flexible to enable local overfitting. In case of a global linear regression, the CoD is suitable, if the number of unknown regression terms is much smaller as the number of available data points. If local regression models are used, as MLS or Kriging the CoD measure usually becomes too optimistic. In cases with significant solver noise, the approximation function may be strongly distorted by local oscillations which imply artificial non-physical correlations. Therefore, measuring the goodness of fit is incapable to avoid the overfitting and hence measuring the forecast quality by means of independent data point sets becomes crucial.

Today, many more meta-model approaches are available and it is often not clear which one is most suitable for a given problem (Roos 2007). Another challenge of meta-modeling is the so-called "curse of dimensionality", meaning, that there is a dramatic decrease in the quality of approximation for all meta-model types as the number of input variables increases. As a result, large number of samples are required to represent high-dimensional problems with sufficient accuracy, having at the same time the tendency to overfit the data as pointed out above. In order to overcome these problems, Dynardo developed the Metamodel of Optimal Prognosis framework (Most and Will 2008, 2011), which will be discussed in a later section. Prior to that, we would like to introduce different strategies of machine learning.

Machine Learning

The machine learning approach can be seen as an extension of the classical response surface methods. Instead of choosing a predefined setup of basis function types and terms manually, this approach tries to learn the complexity of the required model type itself. The type of this automated learning now distinguishes between the different levels of machine learning.

In the **unsupervised learning** so-called unlabeled data, which contain only the information about the input values, are considered. In clustering approaches for example, this may help to find different regions in the variable space, where different data clouds are available, which might be treated differently. On the other hand, dimension reduction techniques are very promising, in cases where a large number of input variables, which show significant local or global dependencies to each other, needs to be considered. Exemplarily, the Principal Component Analysis method or related series expansion approaches are mentioned, which are very efficient to reduce a large input dimension to a few representative variables. Reduction strategies used in Statistics on Structures (SoS) can be labeled as unsupervised machine learning.

In the **supervised learning approach**, the labels of the data, often understood as response variables, which describe a phenomenon depending on the input variables, are represented by a set of mathematical surrogate functions. During the learning or training process, the complexity of the function set is automatically adjusted to the requirements represented by the data. For example, the Support Vector Classification and Regression, which uses local basis functions similar to Kriging, reduces the set of relevant basis terms automatically to these support points, which are required to build the class separation or the response function sufficiently. This case is an example for automatic selection of necessary data points. In the chapter "Metamodel of Optimal Prognosis" Dynardo's MOP technology is introduced and discussed as supervised machine learning approach with the focus on detecting the most important input variables as well as suitable regression functions.

Reinforcement learning approaches differ from supervised learning by the presence of labeled input/response pairs, and by sub-optimal pairs not being explicitly corrected. Instead the focus is on finding a balance between exploration (of uncharted input territory) and exploitation (of current meta-models about input response correlation). Therefore, adaptive strategies are used to add additional support points in uncharted areas, respectively areas of interest to improve the forecast quality of meta-models. Dynardo's Adaptive Metamodels of Optimal Prognosis (AMOP) can be classified as a reinforced learning strategy.

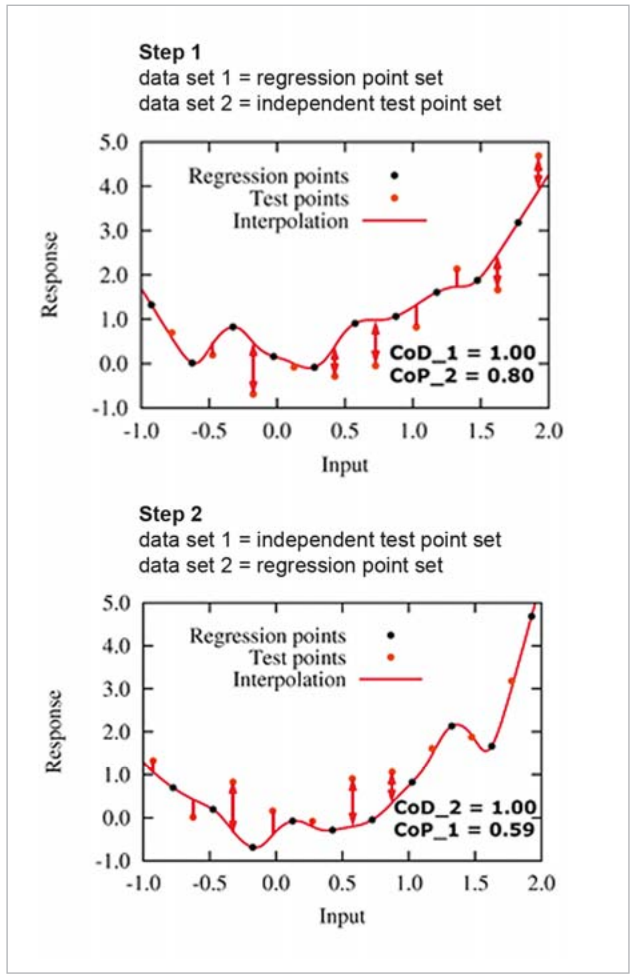

Fig. 3: The Coefficient of Prognosis as measure of the prediction quality based on independent test data points

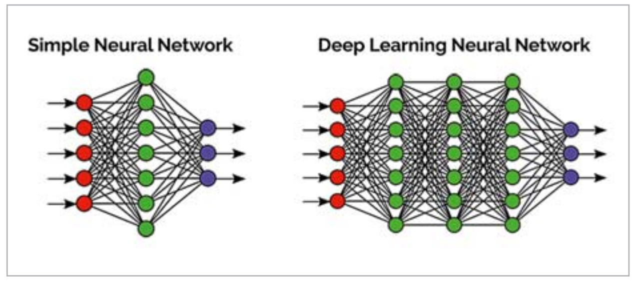

Fig. 4: Simple feed-forward neural network consisting of one hidden layer and deep learning network with several hidden layers

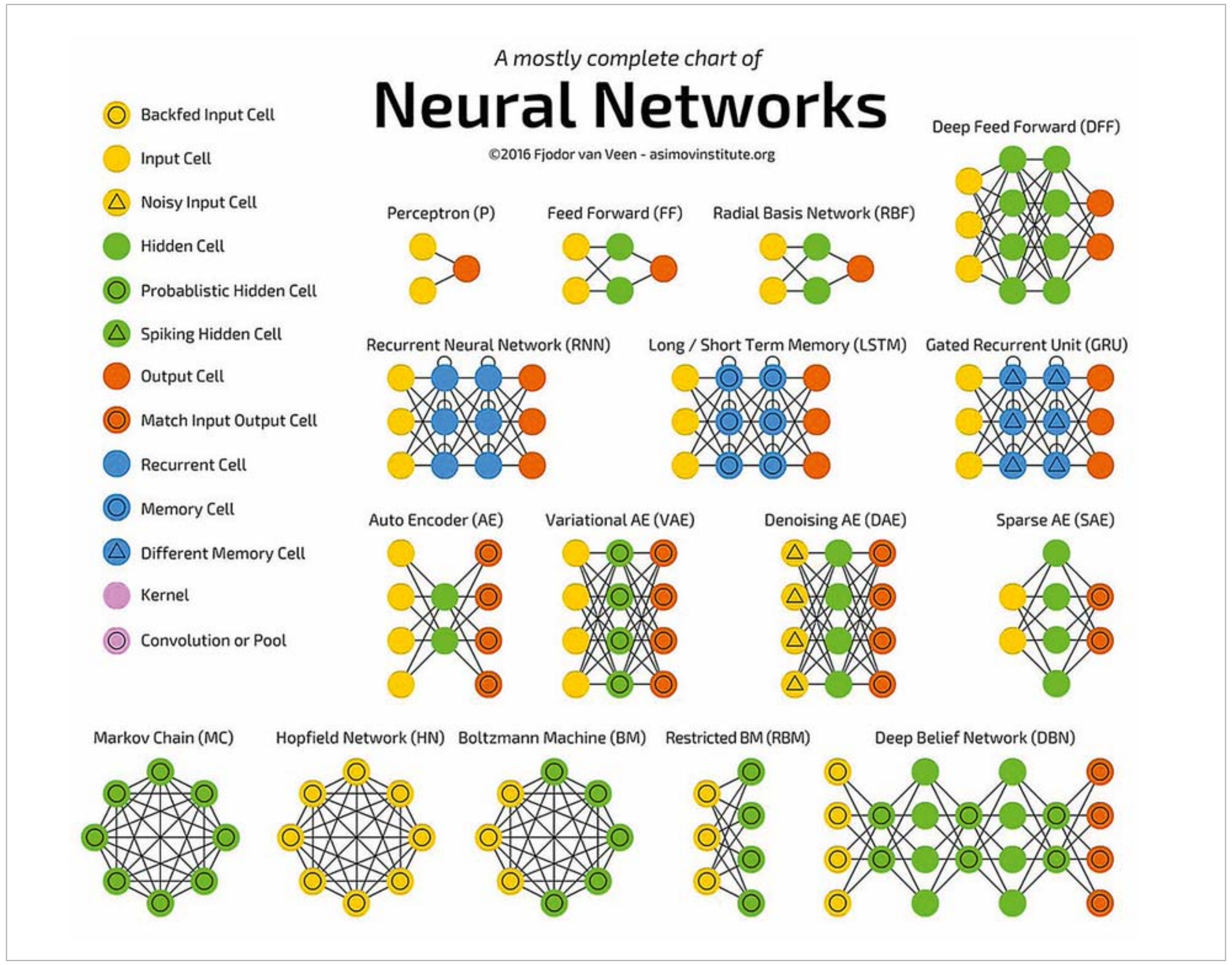

Fig. 5: Typical neural network types and architectures (Source: Fjodor van Veen, Asimov Institute, 2016)

Metamodel of Optimal Prognosis

The Metamodel of Optimal Prognosis (MOP, Most & Will 2008, 2011) can be seen as an advanced machine learning approach with automatic feature detection. Based on the Coefficient of Prognosis (CoP), which measures the forecast quality of an approximation model instead of the goodness of fit, the MOP approach evaluates different regression methods with different basis terms. Based on advanced filter strategies, different input variable combinations, which span different subspaces, are analyzed for different available regression model types. As a result, the optimal input variable set including the optimal approximation technique is obtained, which reaches the largest CoP value for a given support point data set.

One key point in this approach is the CoP, which allows to quantify the prediction quality of the approximation model independently of the model type. This measure is applicable also for interpolation models with perfect goodness of fit. The CoP estimates the fraction of explained variation in the prediction of the model. The residuals are calculated by using an independent test point set to estimate the approximation errors at test points. Based on the cross-validation principle, the prediction residuals are obtained for each data point set by a systematic exchange of regression and test points. With help of this procedure, an automatic selection of regression model types and variable subspaces is possible within the machine learning process.

Figure 3 shows a data set, which is splitted 50/50 to test and regression points in case 1 and vice versa in case 2. Unless advanced regression models are able to show a perfect fitting quality (CoD), the forecast quality (CoP) quantifies the true ability of the models to represent the data set response value variation. The difference between CoD and CoP quantifies the overfitting. It should be noted that in the test case 23% of artificial noise is represented. By using more data points, the CoP measure of any representative spit will converge to 77%.

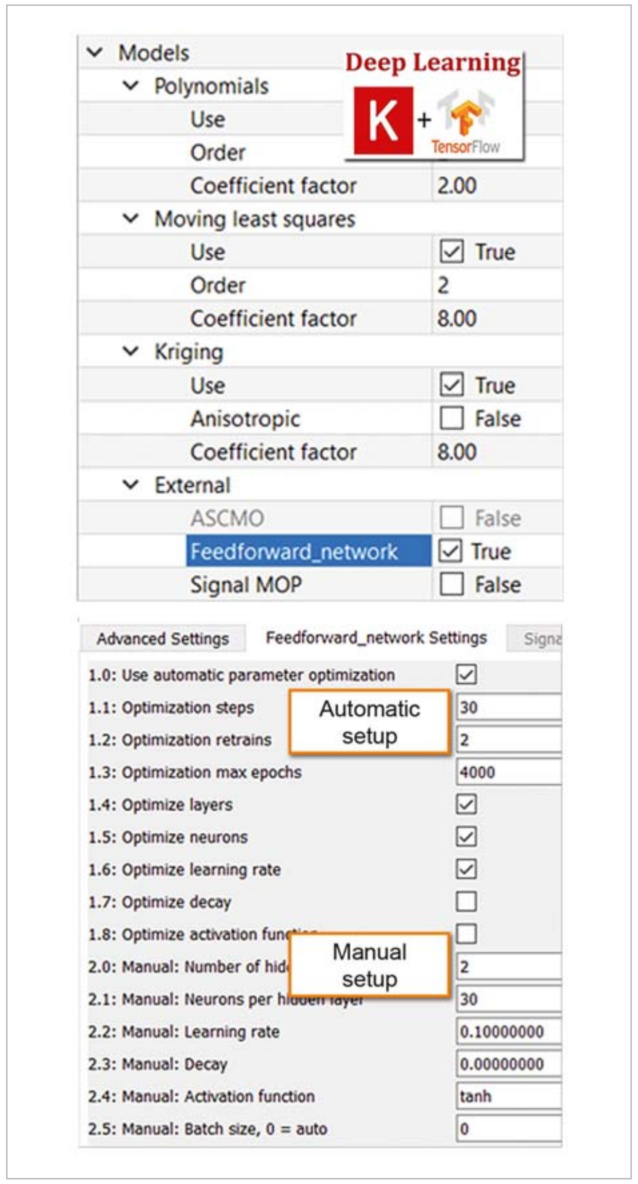

Fig. 6: Set up of optiSLang Deep Learning Extension models in the MOP settings (top: selection of feed-forward model for the MOP competition, bottom: automatic and manual network setup)

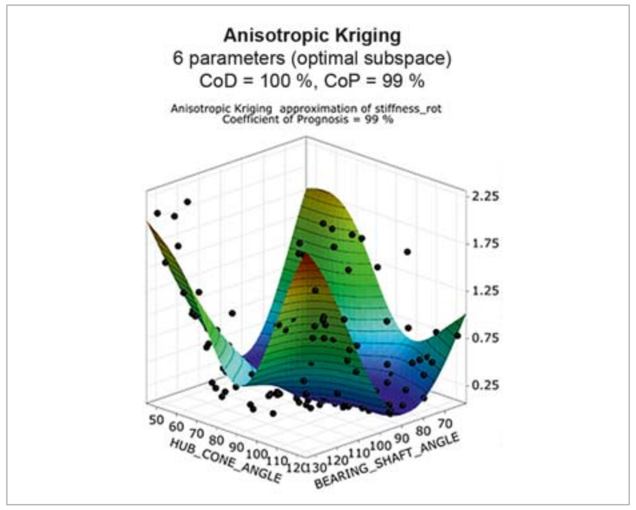

Fig. 7: Rotational stiffness of a turbine impeller approximated by Kriging

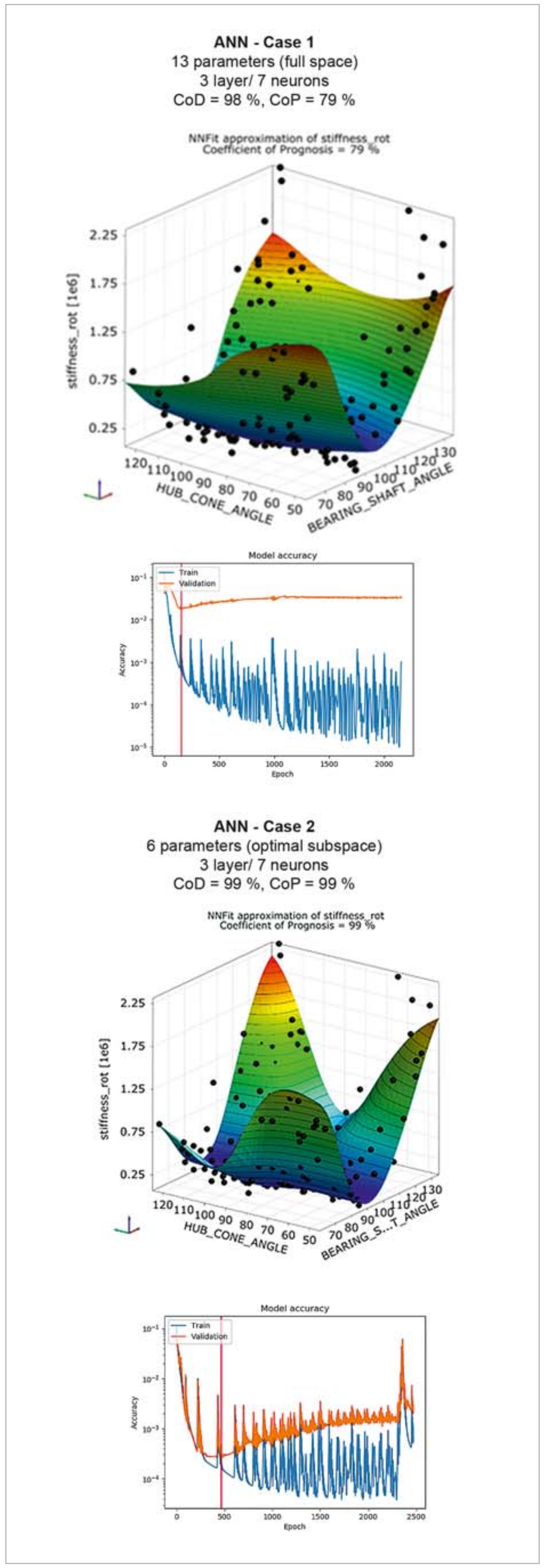

Fig. 8: Rotational stiffness of a turbine impeller approximated by a feed-forward network within the full parameter and the reduced optimal parameter space

Samples	Kriging		Deep Learning Extension		
	Training	CoP	Hidden neurons	Training	CoP
100	2 sec	99.99 %	3 x 10	3 min	99.73 %
500	3 min	99.99 %	3 x 20	7 min	99.96 %
2000	330 min	99.99 %	4 x 30	12 min	99.98 %
10000	not possible		4 x 50	72 min	99.99 %

Table 1: Comparison of numerical performance between Kriging and neural networks on a five-dimensional analytical benchmark function using computation on CPU only

Artificial Neural Networks and Deep Learning

Artificial neural networks are a special type of machine learning methods, which mimic the learning process of the human brain: based on simple neuron activation functions, sophisticated phenomena can be learned just by increasing the complexity of the network with more and more neurons and connections. So-called deep learning neural networks consist usually of several layers of neurons with nonlinear activation functions, whereby each neuron of each layer is itself connected to all neurons of the previous and the following layer. With increasing number of neurons, the complexity of the overall surrogate function increases significantly. Since the training algorithms are mainly based on simply update rules using stochastic optimizers, even such sophisticated deep learning networks can be efficiently trained. Especially, during the last ten years, the efficiency of the training methods could be improved dramatically. This opened the door for more and more complex network types and architectures and therefor for more applications.

In comparison to classical regressions methods, whose number of data points usually increases the training effort exponentially, the training of deep learning networks is still efficient for large data sets. Due to the simplicity of the training, parallelization techniques can be applied easily.

In cases of a sufficient amount of data, a deep learning network structure is able to detect important features itself automatically during the training procedure. In opposite cases, where the amount of data is limited, the reduction of input variables to only the important subset in the MOP workflow can significantly improve the approximation quality of a neural network similarly to classical regression methods. Usually, in such cases, the different approximation models show a similar performance. In our experience, the deep learning networks are a very powerful extension to the classical regression methods, especially if large amount of data are available.

optiSLang's Deep Learning Extension

With the optiSLang deep learning extension, deep learning neural networks can be considered in the model testing process of the Metamodel of Optimal Prognosis. Based on the CoP, the available models are tested and compared. Finally, the best model type is selected. Especially, for large data sets with more than 1000 samples, a significant speed up for the training is possible compared to classical methods as Kriging. Actually, the deep learning extension contains feed-forward deep learning models with automatic configuration of the network topology. Within the extension, the analyzed different model architectures are initialized and trained using the Tensorflow library, which can be efficiently parallelized on CPU and GPU environments.

Example

The rotational stiffness of a turbine impeller was analyzed. Therefore, 176 samples of a Latin Hypercube Sampling with 13 geometry parameters as inputs have been considered. The response values, as rotational and axial stiffnesses as well as performance measures like isotropic efficiency and mass flow and even life time estimates have been obtained for each parameter combination by a time-consuming multi-disciplinary analysis including computational mechanics, fluid dynamics and fatigue analysis. That industrial example was used to test the performance and accuracy of the optiSLang deep learning extension. In Figure 7 the reference solution using the MOP dimension reduction and Kriging approximation is shown. The best possible global forecast quality is 99%. In Figure 8 the approximation functions for the rotational stiffness are shown for a neural network approximation considering all 13 parameters on the first case and only the most important 6 geometry parameters in the second. In case one Figure 8 clearly indicates that the highly nonlinear behavior of the response cannot be represented sufficiently. Due to the flexibility of the model, the accuracy of fit, measured by the CoD, is almost perfect, while the forecast quality, quantified by the CoP, is significantly less. Consequently, the deep learning training, which uses early stopping based on a validation data set to avoid overfitting, results in a rather weak trained model in the full space. This phenomenon is critical especially for smaller data sets. In such cases the automatic variable filtering of the MOP approach is very promising, as shown in this example. The forecast quality could be increased from 81% to 98% by training the neural network with the same topology but in the reduced optimal subspace.

As already pointed out in chapter "Artificial Neural Networks and Deep Learning", in case of small data sets

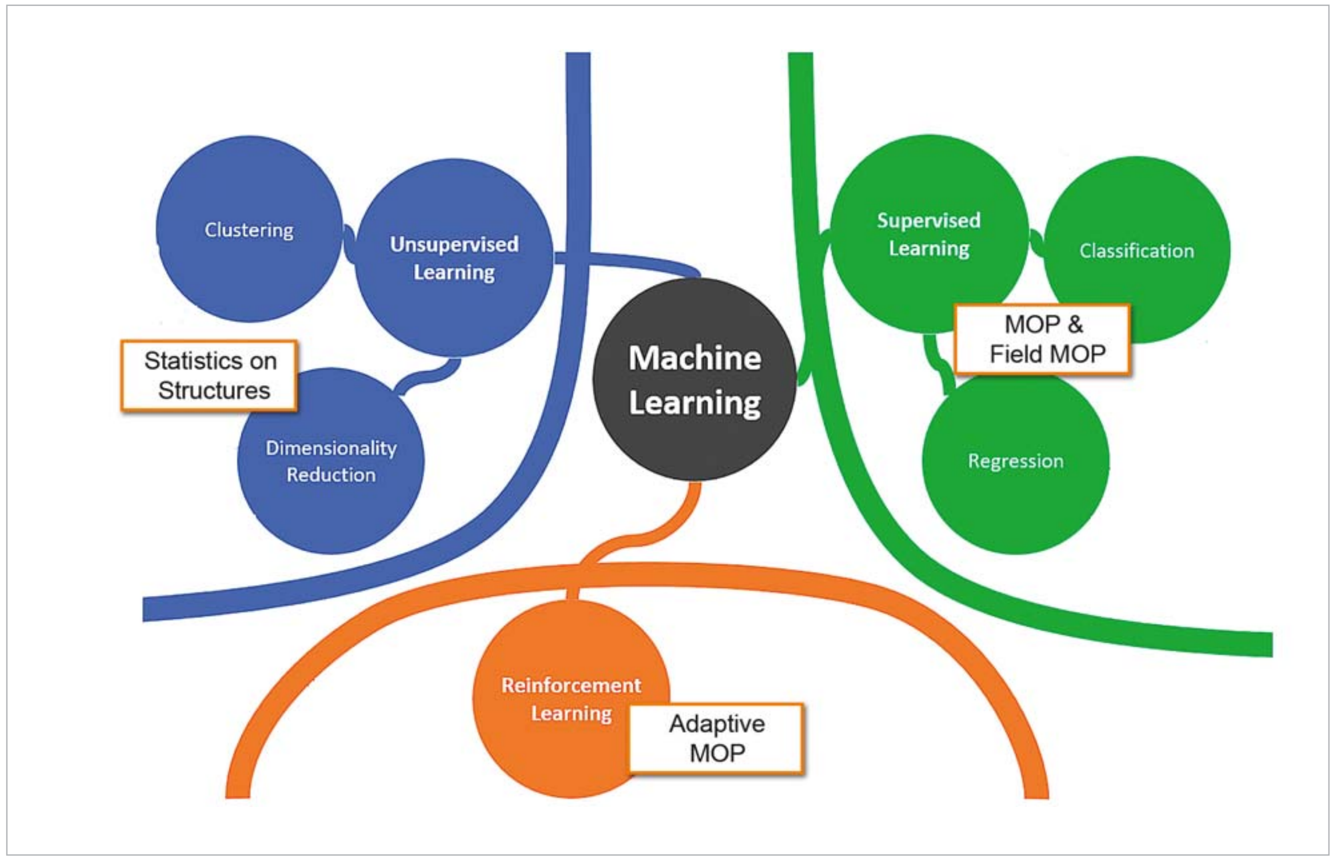

Fig. 9: Representation of different types of machine learning in dynardo technology (Source: www.morethandigital.info)

(50...200) the AI-based deep learning networks show a similar performance to MLS or Kriging in the MOP workflow. In our experience, the deep learning networks become a very powerful extension to the classical regression methods, especially if large amount of data are available. Table 1 (see previous page) shows the comparison of numerical performance using a five-dimensional test example of a non-linear function. It can be clearly seen, that Kriging, which is able to reproduce the nonlinearity, will fail because of its numerical effort when the available numbers of sample rise.

Summary

This article discussed the relevance of "new" AI-technologies in the context of CAE applications. Fortunately, the CAE community in case of AI-based machine learning algorithms can take benefit of the enormous investments over the last decade in implementing public available libraries like TensorFlow from Google or Microsoft Cognitive Toolkit into CAE software applications. The article discusses in detail the MOP framework as supervised machine learning approach and the integration of feedforward neural networks into the MOP competition for the best possible meta-model. Within the MOP workflow, overfitting by using ANN is avoided due to rigorous testing of the forecast quality with help of the CoP. Users can investigate and quantify the global and local forecast quality of an ANN directly in comparison to classic meta-modeling techniques. The interfacing of external machine learning algorithms to the MOP workflow is open to any third-party machine learning algorithm.

Right now, we are working on extensions to non-scalar meta-models, which will open the competition to Dynardo internal solutions for field MOP using Statistics of structures (SoS) as well as to adaptive scalar and field meta-modeling techniques to improve meta-modeling quality by optimally placed additional simulated data points (Adaptive Metamodel of Optimal Prognosis, AMOP).

Authors //
Thomas Most, Johannes Will, Jonas Rotermund, Lars Gräning (Dynardo GmbH)

References

D. C. Montgomery and G. C. Runger (2003). Applied Statistics and Probability for Engineers. John Wiley & Sons, third edition

Most, T. and J.Will (2008). Metamodel of Optimal Prognosis - an automatic approach for variable reduction and optimal metamodel selection, Proceedings Weimarer Optimization and Stochastic Days 5.0, Weimar, Germany

Most, T. and J. Will (2011). Sensitivity analysis using the Metamodel of Optimal Prognosis, Proceedings Weimarer Optimization and Stochastic Days 8.0, Weimar, Germany

Roos, D., T. Most, J. F. Unger, and J. Will (2007). Advanced surrogate models within the robustness evaluation. Proceedings Weimarer Optimization and Stochastic Days 4.0, Weimar, Germany

Russell & Norvig (2009). Artificial Intelligence: A Modern Approach. Prentice Hall

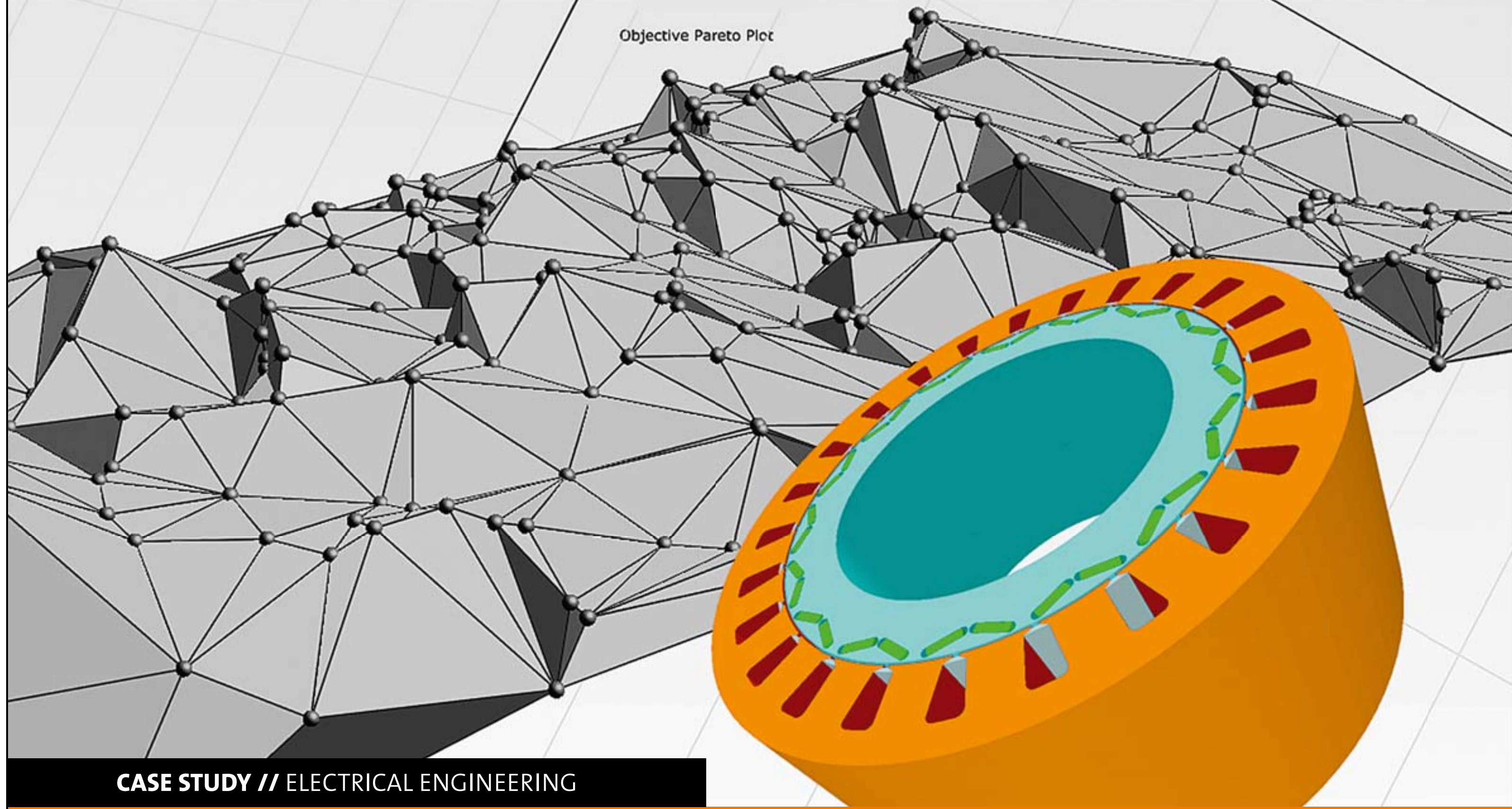

CASE STUDY // ELECTRICAL ENGINEERING

MULTI-CRITERIA ELECTRIC MACHINE DESIGN WITH MOP-BASED PARETO OPTIMIZATION

Experts at Motor Design Ltd demonstrate how the combination of Motor-CAD and optiSLang facilitates a data-driven exploration of the electric machine design space for an EV application utilizing multi-physics simulation.

Introduction

The team of electric machine design experts at Motor Design Ltd. (MDL) in Wrexham, UK, develops the software Motor-CAD consisting of highly efficient motor modeling and simulation tools able to represent besides the electromagnetic facet also the thermal and mechanical properties. The program component Motor-CAD Lab can take in data from all the multi-physical sub-models and based on generating reduced-order models (ROMs) for crucial machine properties (like dissipation through hysteresis in ferromagnetic material and magnetic saturation) entire performance maps can be generated in minutes.

The MDL team around founder Dave Staton and development head James Goss represents decades of experience in academia and industry. It is interesting to reflect how the introduction of optiSLang impacts on the approach to ab initio motor layout. Usually, several basic setup decisions were taken in steps based on simple preliminary calculations, e.g. axial length of the machine, numbers of poles, of slots, of winding turns. Only after fixing that frame, algorithmic optimization was applied further downstream. It is clear that suboptimal decisions taken at the preliminary framing stage can set the entire motor layout procedure on a wrong track. With its automation and sensitivity analysis capabilities, optiSLang brings within reach to greatly systematize and objectivize the entire ab initio machine layout procedure.

This case study outlines the current evolution state of a compressed layout procedure of a permanent magnet synchronous machine intended for use in a plug-in hybrid car, and it shows how automated step-wise model building and MOP-based Pareto optimization are leveraged to ensure a real wide-angle exploration of the available design space, i.e. to avoid premature frame-narrowing.

The machine model

The chosen motor type and topology is a permanent magnet synchronous machine. The embedded magnets in the rotor are ordered in V-shaped pairs to form a pole. This is a well-known design since it was invented by Toyota for the first generation Prius. Figure 1 (see next page) shows the cross section geometry of the 24-slot 16-pole motor. The numbers of slots and poles are indeed kept fixed, but the number of turns of the winding and the axial length of the machine are defined as variables, and they are subject to the overall optimization procedure.

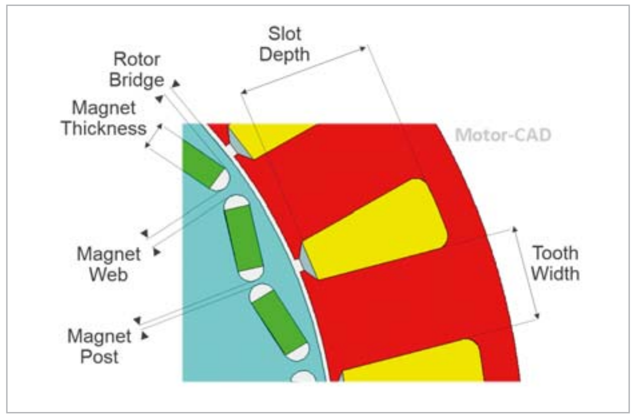

Fig. 1: Motor cross section geometry: Slot Depth Ratio = Slot Depth / (Slot Depth + Stator Back Iron Thickness) | Slot Width Ratio = Avg. Slot Width / (Avg. Slot Widt + Stator Tooth Thickness | Split Ratio = Stator Inner Diameter / Stator Outer Diameter

The introduction of three dimensionless split ratios for (1) slot width, (2) slot depth, and (3) stator-vs-rotor size ensures that (a) there is by principle no infeasible geometry and (b) extremely different setups can be reached by allowing broad ranges for all parameters. All flexible cross section geometry parameters together with the variable active length form a nine-dimensional parameter space.

Actually, no parameters describing electric circuitry or electric driving conditions are subject to variation. The reason is two-fold: on the one hand the main capability properties of the power electronics are considered as given boundary conditions, on the other hand the scripted recipe for single design evaluation together with Motor-CAD-internal routines allows the evaluation procedure to flexibly adjust the winding setup so it optimally conforms to the limits imposed by the power electronics while ensuring a realistic slot fill factor, current density, and cooling properties.

What does the scripted Motor-CAD machine model evaluation look like? Figure 2 shows a schematic of the sequence of analysis steps. Three aspects are particularly noteworthy: (a) the script avoids complete evaluations of motor designs which fail to meet a basic peak torque requirement; (b) scaling for winding turns avoids burdening the analysis with discrete parameters and combinatorial rules or with nested optimization; and (c) in the main part of the script the design evaluation expands the scope beyond selected operating points towards a complete duty cycle. This is made possible by the Lab component of Motor-CAD.

The Lab module utilizes the multi-physics solvers in Motor-CAD. It combines an efficient electromagnetic ROM building method with fast-solving lumped-parameter thermal models and control strategy algorithms. This enables a rapid characterization of the electric machine across the full operating range.

Figures 3 and 4 depict some of the main outcomes of the Lab-based machine analysis exemplarily for one of the optimized designs discussed below. Figure 3 shows the torque-speed envelopes for peak and continuous operation. During peak performance the heat generation in the machine is far

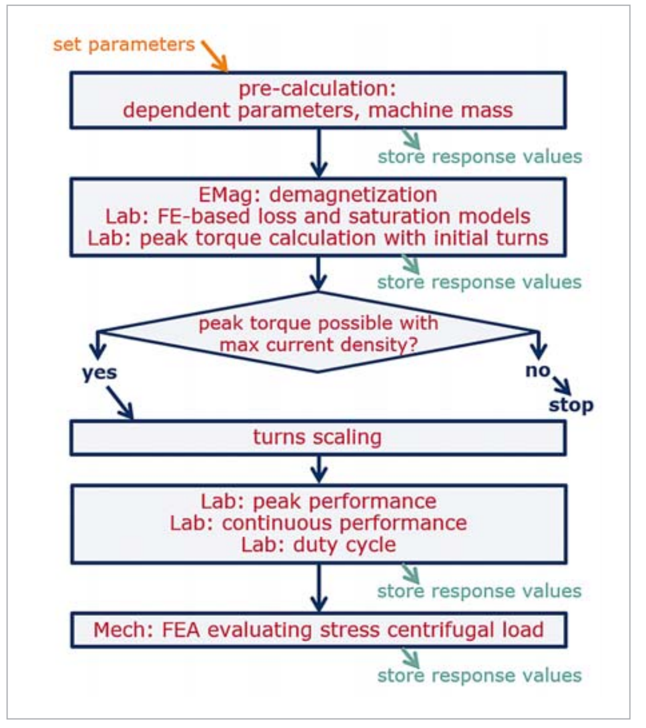

Fig. 2: Schematic of scripted Motor-CAD evaluation of one single design

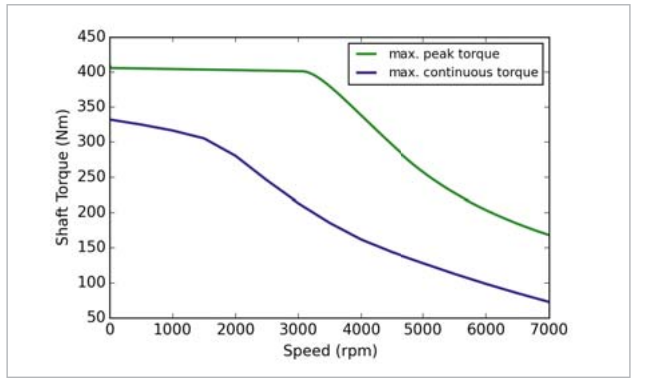

Fig. 3: Short-term and continuous performance envelopes

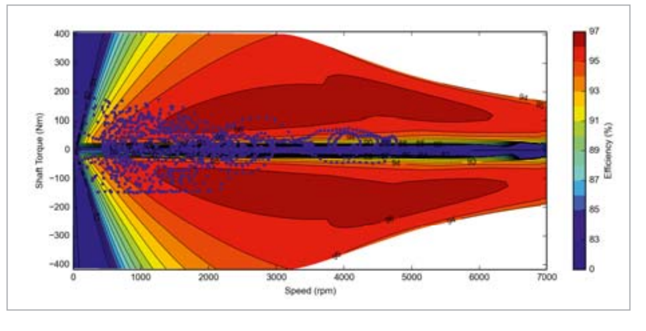

Fig.4: Efficiency map with overlaid WLTP-3 duty cycle

beyond the cooling capacity. The characteristic line of peak performance shows operating points which can be upheld for short time periods, typically up to 30 seconds. The continuous performance curve represents the envelope of all operating points within the machine's thermal limit, i.e. all feasible steady-state operating points where the dissipated

Total effects

Models \ Parameter	i_Active_Length	i_Bridge_Thick	i_Mag_Pole_Angle	i_Mag_Post	i_Mag_Thick	i_Mag_Web	i_Slot_Depth_Ratio	i_Slot_Width_Ratio	i_Split_Ratio	Total
o_Wdg_Mass	6.7 %	0.0 %	0.0 %	0.0 %	0.0 %	0.0 %	16.7 %	19.2 %	60.5 %	100.0 %
o_Torque_Ripple_500rpm	3.4 %	4.8 %	11.7 %	14.3 %	4.6 %	22.1 %	16.6 %	2.8 %	34.0 %	93.1 %
o_Torque_Density	100.0 %	0.0 %	0.0 %	0.0 %	0.0 %	0.0 %	0.0 %	0.0 %	0.0 %	100.0 %
o_Stress_Safety	0.0 %	13.4 %	34.1 %	0.3 %	0.5 %	4.8 %	0.1 %	0.0 %	46.5 %	97.6 %
o_Stator_Core_Mass	26.2 %	0.0 %	0.0 %	0.0 %	0.0 %	0.0 %	3.3 %	8.6 %	62.4 %	100.0 %
o_Rotor_Core_Mass	33.0 %	0.0 %	0.9 %	0.2 %	3.9 %	1.0 %	0.0 %	0.0 %	60.7 %	100.0 %
o_Peak_Power_Max	5.4 %	3.9 %	11.4 %	6.6 %	0.0 %	5.7 %	7.2 %	0.1 %	61.3 %	99.4 %
o_Peak_Power_6krpm	6.3 %	4.7 %	12.2 %	9.1 %	0.0 %	7.0 %	6.8 %	0.4 %	58.3 %	99.2 %
o_Magnet_Mass	26.7 %	0.0 %	13.9 %	0.6 %	17.2 %	14.3 %	0.0 %	0.0 %	31.4 %	100.0 %
o_Eff_WLTP3	9.3 %	3.9 %	21.6 %	12.7 %	7.8 %	13.2 %	20.3 %	8.9 %	24.3 %	98.4 %
o_Cont_Torque_5krpm	7.7 %	2.7 %	13.3 %	6.7 %	0.0 %	16.2 %	8.0 %	0.0 %	45.9 %	98.9 %
o_Cont_Torque_1krpm	45.6 %	4.3 %	14.9 %	7.6 %	2.7 %	7.2 %	1.3 %	1.3 %	14.6 %	98.2 %

Fig.5: CoP matrix

power does not exceed the capacity of the cooling system.

The performance map in Figure 4 shows motor efficiency in the top half and generator efficiency in the lower. It is based on the "max torque per ampere" strategy of optimal operation point choice. The overlaid set of blue dots symbolizes the WLTP-3 driving cycle. Judging the overall efficiency subject to a realistic drive cycle is very valuable because it does not help to offer few perfectly efficient operating points if they are rarely ever reached and exploited by any vehicle on real-world roads. The overall drive cycle efficiency is calculated by integrating over all phases of motor as well as generator usage.

As a last step of evaluating one machine design, the newest Motor-CAD component is used for conducting a finite element analysis (FEA) of structural mechanics for calculating material stress in the rotor and deducing a safety factor of structural integrity under the centrifugal load at 120% overspeed.

Meta-model-based sensitivity analysis and optimization

With the scripted analysis routine as outlined above, Motor-CAD is used to establish a full machine characterization for every demanded design variation in a few minutes. From each analysis step the characteristic key values are collected in optiSLang for the generation of a comprehensive set of response surfaces, which offers – if good enough by CoP – the potential to conduct the entire design space exploration and optimum search on one single MOP in one run.

After conducting an advanced Latin hypercube sampling (LHS) design variation study of 400 points, 14 designs were sorted out for failing to meet basic torque requirements, leaving 386 useful designs for entering the database for meta-modeling. Figure 5 shows the CoP matrix associated to the MOPs for all optimization-relevant response quantities. On this database, the settings (1) dimension reduction not allowed, (2) anisotropic Kriging included, and (3) CoP tolerances at zero were able to yield for several quantities the best MOP judging not only by the total CoP number, but also comparing point distributions in the residual plots visualizing cross-validation errors. If e.g. a quantity like torque is intended for maximization, then the model fit around the upper data ranges is of course more relevant than towards lowest values. This is how the residual plot may justify a preference even when total CoP values of available MOPs are very similar.

The high total CoP values of generally >97% show that for most responses only a tiny fraction of the variance remains unexplained by their meta-model, which represents ideal preconditions for MOP-based optimization. Only for the quantity characterizing torque ripple the CoP value of 93% is substantially lower. This is not surprising. Torque ripple is due to the tangential component of the magnetic field across the airgap between rotor and stator. The torque effect is created by the integral all around the circumference. Generally, when integral quantities are derived from manifold spatial patterns a high amount of information is lost and the response behavior is hard to relate to the input parameters causing specific pattern expressions.

Exploiting the MOP for finding the optimal motor design

Due to the high CoP values testifying that most of the system behavior was captured, the set of MOPs offers itself for optimization and answering what-if questions in the form of experimenting with different combinations of objectives and constraints. Too sharp constraints make the problem solution impossible, but too weak constraints will allow

Name	Type	Expression	Criterion	Limit	Evaluated expression
constr_Cont_Torque_1krpm	Constraint	o_Cont_Torque_1krpm	≥	315	349.671 ≥ 315
constr_Cont_Torque_5krpm	Constraint	o_Cont_Torque_5krpm	≥	124	158.852 ≥ 124
constr_Peak_Power_Max	Constraint	o_Peak_Power_Max	≥	120	146.288 ≥ 120
constr_Peak_Power_6krpm	Constraint	o_Peak_Power_6krpm	≥	100	136.27 ≥ 100
constr_Stress_Safety	Constraint	o_Stress_Safety	≥	1.5	1.9215 ≥ 1.5
obj_Efficiency_WLTP3	Objective	o_Eff_WLTP3	MAX		-93.4978
obj_Active_Volume	Objective	400/o_Torque_Density	MIN		17.8599
constr_Torque_Ripple_500rpm	Constraint	o_Torque_Ripple_500rpm	≤	10	10.8724 ≤ 10
obj_Material_Cost	Objective	8*o_Wdg_Mass+80*o_Magnet_Mass +1.04*(o_Stator_Core_Mass+o_Rotor_Core_Mass)	MIN		298.728

Fig. 6: Optimization criteria

the algorithms to finish with not quite competitive designs. As no simulations are necessary, these valuable what-if tests for the purpose of orientation in the design space are generally quick to conduct. In this case study, after going through a few setup alternatives, the set of criteria with three objective functions depicted in figure 6 was found to be challenging while at the same time yielding the well-interpretable Pareto front of highly competitive designs shown in figure 7.

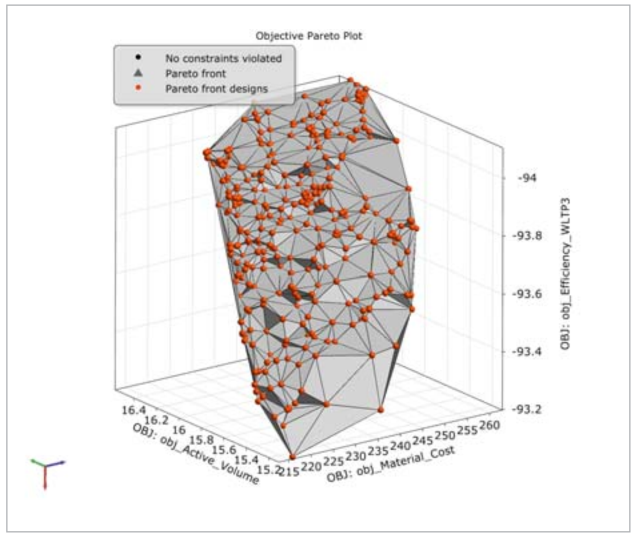

Fig. 7: Pareto front as result of running an evolutionary algorithm (EA) on the MOP

While the trade-off between the motor efficiency and its volume is directly revealed by the Pareto surface in the 3D space, the dependency on the material cost (volumes times price of steel, copper & magnet) seems little and the surface appears almost flat in that direction. By taking the cost parameter as constraint instead of objective, it is possible to generate linear Pareto front structures in a 2D objective space. A plot compiling five such Pareto fronts from independent evolutionary algorithm (EA) runs is depicted in figure 8, and this finally reveals the well-known engineering goal conflict for permanent magnet motors, that extremely high torque and efficiency performance in combination with small motor size can only be reached by increasing the cost-driving content, the rare-earth magnets.

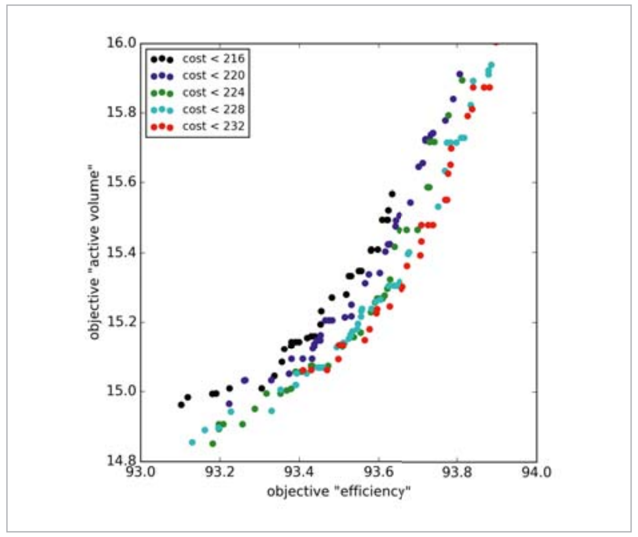

Fig. 8: Set of several two-objective Pareto fronts

The Pareto fronts in figure 8 contain between 34 and 51 designs, each front being the result of an EA run consuming around 10^4 MOP function calls. It is clear that continued evolutionary optimization will be able to resolve the Pareto fronts more and more finely and push the structures forward by a few more increments. Based on a MOP solver the exercise does not have to be computationally burdensome. However, as the tendency caused by the cost limit has already become apparent, and as a small and well-defined set of characteristic designs is most of the time preferable over a large set of stochastic designs, this case study concludes by presenting a final stage of single-objective optimization (SOO) runs: Just as the cost parameter was transformed from objective into limit to get from figure 7 to 8, the transformation of the motor volume from objective into constraint yields a single-objective criteria set allowing the use of efficient deterministic optimizers and allows to achieve the series of optima added into the objectives plot of figure 9. Based on two selected steps of the cost limit and three steps of the volume limit (dashed grey lines), and feeding it with a constraint-fulfilling Pareto-efficient start design, optiSLang's ARSM algorithm was run six times and yielded six converged solutions. These six quintessential parameter combinations were finally validated by conducting additional full Motor-CAD evaluation of the designs. The simulation outcomes in terms of the two Pareto objectives "efficiency" and "volume" are appearing as "validator" points in figure 9. Analog to being right on the limit in terms of "volume" (visible) the points were pushed right onto the "cost" limit (not depicted) by the optimizer. In terms of "efficiency" there is a visible small offset between the MOP-based ARSM optima and the validator points which reminds that any MOP is only an approximating model. In terms of "cost" and "volume" the validator offsets were found to be quite infinitesimal which can be attributed to the little complexity of the quantities going into these objectives. From these six designs the one with cost < 224 and volume < 15.3 is furnishing the plots in figures 3 and 4.

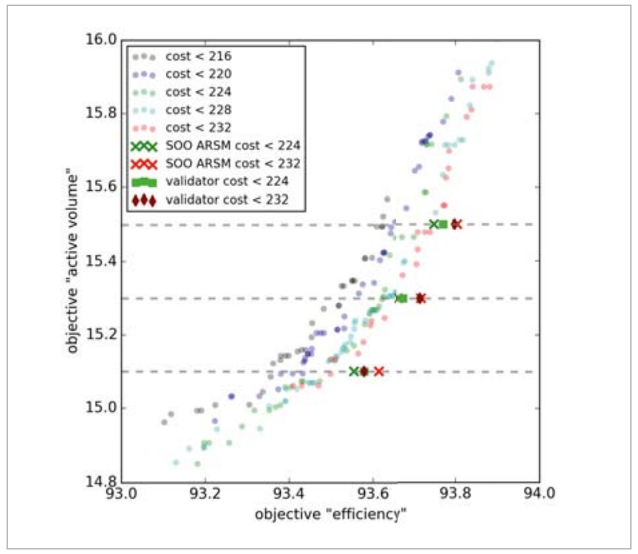

Fig. 9: Validator designs added to the Pareto front plot

Summary

The case study presents a parametrized permanent magnet motor model and outlines its script-driven electromagnetic, thermal, and performance map evaluation in Motor-CAD. This machine simulation setup allows a full optimal layout procedure based on one step of sensitivity analysis and one step of MOP generation. Insight-seeking exploration of a very broad design space and (more or less) constrained optimization can all be conducted on Metamodels of Optimal Prognosis. Conscious steps of constraint sharpening, Pareto front generation, and deliberate trade-off solution choice are outlined. The intention is to show how benefiting from efficient Motor-CAD modeling techniques in combination with optiSLang algorithms and automation features enables to progress the best practice for ab initio electric machine layout towards fewer decision points and greater objectivity.

Authors // Nicolas Rivière, James Goss (Motor Design Ltd.), Markus Stokmaier (Dynardo GmbH)

MODELING TEST RIGS FOR AIRPLANE HIGH-LIFT SYSTEMS BY DATA-BASED MODELS

Airbus and Dynardo are developing Data-based models for dynamic systems to be used in real-time tests. The aim is a decisive contribution to the digitization of work processes and an increasing efficiency in development and testing.

Aircraft High-Lift System

The High-Lift System (HLS) of an aircraft has the task of generating additional lift in various flight phases. In aircraft development, on the one hand, it has to be designed for optimum take-off and landing behavior, and on the other hand it has to offer the lowest possible air resistance during the flight phase. In addition to aerodynamic efficiency and flight performance, functional safety is a key development criterion.

Fig. 1 shows the control of the leading edge panels (slats) and trailing edge panels (flaps). The commanded position is transmitted from the cockpit via the Slat Flap Control Computers to the drive units of the transmission system for the slats and for the flaps. This means that the flaps on both wings are usually moved symmetrically.

High-Lift Test Center in Bremen

Since the beginning of the A380 high lift testing in 2001, the Airbus High-Lift Test Center is based in Bremen. In a 10.000 sqm hall, high lift systems for all Airbus A/C models are tested. The main activities of the High-Lift Test Center in Bremen are the integration of the HLS on test rigs, the implementation of the HLS certification test program and the execution & analysis of the necessary tests for release of the HLS for the “First Flight” and for “Entry into Service”.

Since 2015, Dynardo, the Airbus High-Lift Test Center and its partners Airbus Group Innovations Hamburg, P3 Group Hamburg and MSC Software Munich have been running research projects to introduce accurate and fast data-based models into virtual test environments. The current project AGILE-VT / ViSA, funded by the Federal Ministry for Economic Affairs and Energy (BMWi) under call no. Lufo 5.3, aims at the advancement of such models for dynamic, interactive application within a real-time environment.

Test Methods

There are different methods in place for the testing of HLS.

1. Physical benches for testing of system components

As shown in Fig. 2, physical benches are used for the certification of high-lift systems. Original components are installed in aircraft-type specific test rigs. The physical benches are also required for later verification of model extensions. To comply with the obligation to provide evidence to the authorities,

Fig. 1: Principle structure of the High-Lift System (HLS)

these tests have to demonstrate that all system requirements have been met. For this purpose an intensive test campaign as part of the type certification is necessary.

The advantages of physical tests are, on the one hand, that the test setup is a representative equivalent of the aircraft and the results obtained are accepted by the authorities. On the other hand, each aircraft-type requires its own highly complex test rig, whose installation and maintenance is very cost & time intensive. Original components must be used

Fig. 2: Test rig of the A380. In the front, drive systems and load cylinders to simulate the air load.

which may not be available during the early development phase. The range of application of physical tests is limited by the mechanical construction; changes of the test rig are only possible by complex reconstructions.

2. Functional models for testing the function and logic of the control computers

Simulators are used to test the HLS control computers in a simulated aircraft environment. Original parts are simulated by software modules. Simplified models can be used for the purely functional simulation, hence detailed modelling of physical behavior must not be considered. This kind of test enables a high degree of automatization and real-time capability, which corresponds to a typical clock cycle of 2ms. Functional or logical tests are conducted that way, e.g. the checking of threshold values, time spans for certain processes, etc..

3. Virtual tests using detailed simulation models

Virtual tests are used, for example, for experiments which cannot be performed on the physical bench. Figure 3 shows

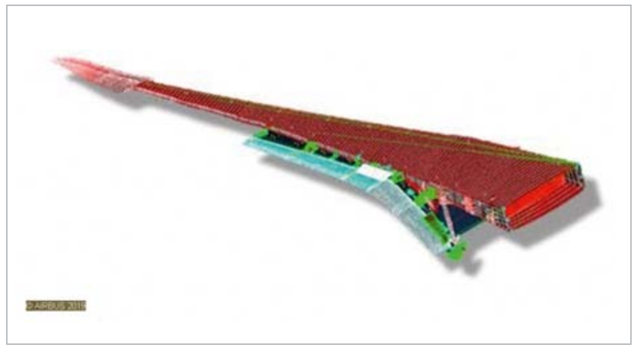

Fig. 3: Model of the A350 wing, simulation of wing bending

an example of a simulation with wing bending (large deformations). Modification of test properties such as stiffness, friction or damping can be easily implemented without rebuilding the virtual test rig. In order to simulate entire motion sequences, the simulation models include both the respective aircraft components and the test rig itself (see Title Image).

Disadvantages of virtual tests are high computing times, which, on the one hand affect the waiting times and on the other hand prevent the real-time capability. A physical reference system is always necessary to verify or optimize the accuracy of the virtual model.

Data-Based Models

In this context, Data-Based Models (DBM) are purely mathematical models for dynamic system reactions, without physical modeling. They thus differ from so-called Reduced Order Models on a physical basis. The DBM are exercised on the basis of given data. In the ViSA project, no real experiments are used for the training, but virtual experiments with a precise simulation of the High-Lift system. This allows a large amount of data for the training and the targeted generation of additional support points in areas where the accuracy must be increased.

Of course, the detailed models must also be able to reproduce the experiment exactly in order to provide high-quality training data for the DBM. It is possible to use parameter identification methods to adapt the detailed models to experimental data so that they deliver the most realistic results possible. However, they are usually much too complex to interact with a test rig in real time. DBM are also advantageous for the investigation of parameter uncertainties or tolerances within the framework of a variance-based robustness analysis. This allows the influences of tolerances or parameters which are difficult to measure (such as damping or friction) on the system behavior to be determined quickly, thus enabling more robust and mature systems to be developed.

A first concept of the DBM was developed in the context of a preceding project [1], [2]. These developments led to the Field Metamodel of Optimal Prognosis (F-MOP), a module of Statistics on Structures (SoS), which can be easily used in optiSLang via the MOP node.

The method of the model approach is to generate a Design of Experiments (DoE) out of the input parameters and to calculate the time series of the responses of the simulation model. The loads of the simulation model are given by the considered virtual experiment. SoS develops the signals by Karhunen-Loève decomposition into a series of invariant form functions scaled by variable amplitudes. The well-known MOP algorithm generates metamodels of the amplitudes depending on the input parameters. The MOP solver, which in turn calls a SoS library, can be used to generate the corresponding signals for new parameter sets within one step. The limitation of this approach, however, is the fixation of the signals over the entire duration of the process. In this sense, the model is static or time-invariant.

In order to integrate the DBM into a system as a component, e.g. to replace part of a test rig as a software-in-the-loop, it must be able to react to changing loads. In addition, the model must also react dynamically to changing parameters for simulating experiments such as artificial actuator failure or wing tip break.

The further development to a dynamic DBM requires a time integration. In the first step, the DBM is again trained on the basis of the transient time series resulting from a DoE of the parameters. Here, unit pulse loads are applied to the simulation model. In a second step, the displacements in the time domain are determined by numerical solution of the Duhamel-Integral. The approach bases on the assumption of any load time series as a chain of impulses. The time series of the displacements result approximately from summation of the impulse responses, starting with the current time step and scaled by the current external load [3]. This solution is valid actually only to linear, time-invariant systems with one degree of freedom. If the system parameters change, the system is no longer in balance. Even though, it is easy to determine the disequilibrium by summing the internal and external forces and to minimize it by simple iteration within the time steps. This allows the dynamic DBM to respond not only to changing loads, but even more to weak non-linearity. The formulation of this balance correction requires an insight into the physics of the system, so it is no longer a purely mathematical model. However, it should be emphasized that this error correction does not consist of a comparison with a reference solution, but is only generated from information provided by the DBM itself. In literature further Duhamel solutions for other differential equations can be found.

During application, usually, one has to deal with multiple degree freedom systems. If there are few excitation points and also the structural responses are to be evaluated at few points, the Duhamel approach can still be used. It can be shown that coupling terms can be considered as single degree of freedom systems, too. The solutions for the respective degree of freedom and coupling effects can be superposed. So, one has to create a corresponding number of DBMs for all combinations of excitation and evaluation points.

Demonstration Example

The effectiveness of the DBM approach will be illustrated using a simple test example. A hydraulic load cylinder with a connected single mass oscillator ("Structure") is considered (see Fig. 4). A force requirement is modified by the cylinder due to internal friction and damping as well as the adiabatic effect and passed on to the single mass oscillator. The feedback of the reaction of the single mass oscillator to the cylinder is effected by displacement and velocity.

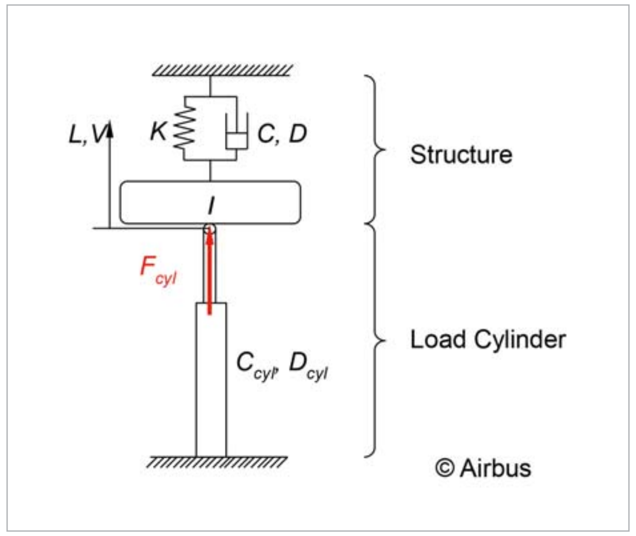

Fig. 4: Demonstration model; component "Structure" is represented by a DBM

The single-mass oscillator is simulated by a DBM that interacts with the load cylinder. For the training of the DBM, virtual experiments with Simulink were performed, varying the system parameters stiffness K, Coulomb's friction C, viscous damping D and mass inertia I. As a test case, a load is applied as a ramp between 0.5 sec and 1.5 sec and removed between 10 sec and 11 sec. In addition, there is a 50% jump in stiffness at 5 sec (see Fig. 5).

The entire system was simulated with Simulink as a reference. To use the DBM, Dynardo's F(ield)-MOP-solver library is linked to Matlab and the interaction between load cylinder and DBM is simulated there. Figures 6 and 7 show the excellent agreement between the reference solution and the dynamic DBM.

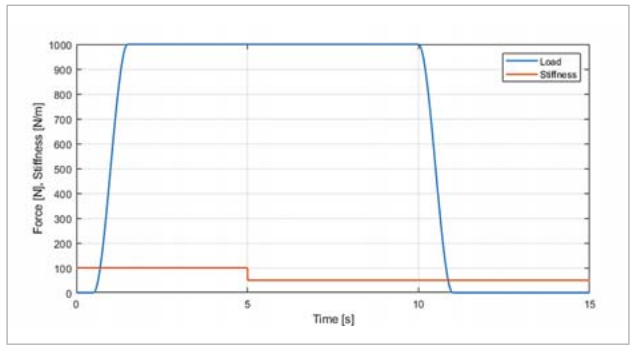

Fig. 5: Transient load on the cylinder and stiffness of the single mass oscillator

Conclusions and Perspectives

Data-based models are able to simulate dynamic structures fast and accurately. In addition to the use of DBM in interaction and thus as an extension of physical or functional experiments, they also enable rapid uncertainty analyses to prove the expected function of components. The models presented here are mathematical in nature, in contrast to e.g. Reduced Order Models. Through the extension by a time integration, the simulation of dynamic structures is possible. The transfer to other physical phenomena, e.g. temperature flow in motors and control units, is supposed to be possible.

In a previous project, data-based models were developed, which were able to simulate the detailed physical behavior of a HLS transmission in connection with model uncertainties (e.g. friction, damping) in the virtual test. The execution speed could be increased by DBM up to real-time, i.e. 500 cycles per second, while maintaining accuracy in comparison with physical tests.

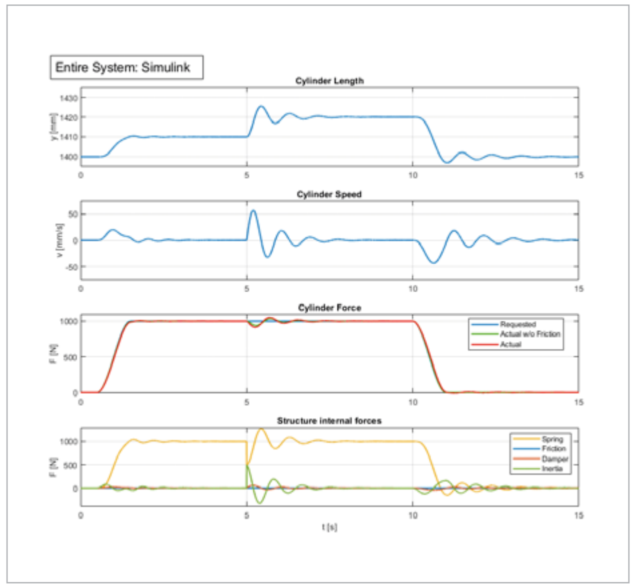

Fig. 6: Reference solution for the complete system consisting of load cylinder and single mass oscillator

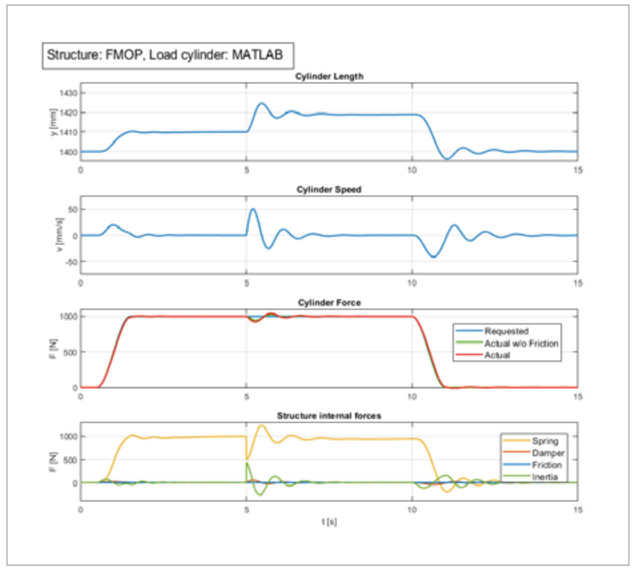

Fig. 7: Simulation of the single mass oscillator as dynamic DBM

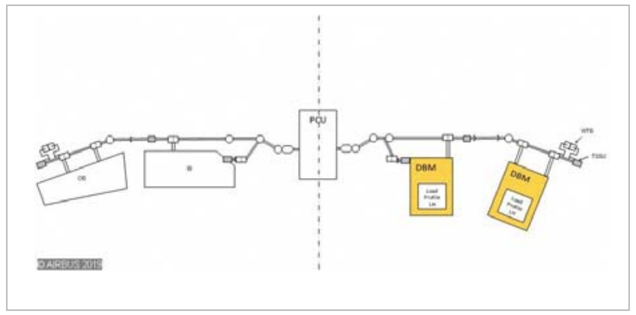

Fig. 8: Use of DBM at the HL test rig

The current project aims at replacement of a physical component at the test rig by a DBM. The behavior of structural components such as landing flaps is to be simulated using DBM on the test rig, Fig. 8. Structural components are required for testing system components. They represent the passive aircraft environment controlled by the system components.

By using DBM in aircraft development, experiments can be carried out much faster and more flexibly. The con struction of the test rig is simplified by simulated structural components and is more flexible for different aircraft types by simply modifying the DBM. Both rig-like and aircraft-like tests are available. The former also serve the planning and validation of physical experiments. Aircraft-like tests can be performed early in the development phase even before original physical components are available. This will significantly reduce development time and offer the opportunity to increase the product maturity.

Authors //
Jürgen Horwege (Airbus GmbH, Bremen)
Veit Bayer (Dynardo GmbH, Weimar)

References

[1] Bayer, V. et al., "Metamodeling of Dynamic Systems used for Virtual Testing", Weimar Optimization and Stochastic Days. Weimar: June 2016.

[2] Bayer, V. et al., "Signal-Based Metamodels for Predictive Reliability Analysis and Virtual Testing", Advances in Science, Technology and Engineering Systems Journal, ISSN: 2415-6698, Vol. 3, No. 1, 342-347 (2018).

[3] Clough, R. W., Penzien, J., Dynamics of Structures. Computers & Structures Inc., Berkeley (USA): 3rd ed. 1995.

Gefördert durch:

Bundesministerium für Wirtschaft und Energie

aufgrund eines Beschlusses des Deutschen Bundestages

CUSTOMER STORY // AUTOMOTIVE ENGINEERING

OPTIMIZATION OF AN ACTUATOR MAGNETIC FORCE WITH OPTISLANG

With a coupling of ANSYS Maxwell and optiSLang, it is possible to obtain geometric improvements of an actuator by optimizing the shape and level of its characteristic force curve.

The system, objective and constraints

With the possibility of combining Maxwell and optiSLang, the optimization expertise can be used to improve actuators for Hilite products. In following, an example will show how the combination of ANSYS Maxwell and optiSLang was used to optimize the magnetic force curves and to improve valve performance and behavior.

Issue

Hilite produces valves for the usage in automatic and double clutch transmissions (DCT). They contain different valves with different tasks, which usually are optimized separately. For future products a new actuator had to be designed that could be used in multiple valves. Two of them are gear shift and clutch control valves; they are shown in Figure 1. Both curves, the one for the pressure in top and the other one for the flow valve in the bottom have to be actuated optimally. Therefore, different criteria of the different valves ensure the possibility to optimize the new actuator and guarantee the functionality at the same time.

ANSYS Maxwell is able to compute magnetic forces, which are part of the main objective of the optimization task. Figure 2 pictures the simulation model that is used to compute the axial magnetic force on the armature. Due to already existing analyses, the number of parameters that mainly influence the force could be reduced to five. All important parameters are located within the same region of the valve. The parameters influence the characteristic curves, which are shown in the figure as well.

Criteria for the optimization

During the development process, the changes in the initial design lead to various optimization tasks. Therefore, objectives, depending on characteristic pressure curves of the system, have been generated. The most important criteria are marked in different colors on the field of characteristic curves in Figure 3. Here, the criteria 1 to 7 are used as constraints to get the curves in the optimal direction. The criterion 8 is set as an objective.

Number 1 (green) is calculated between two specific stroke positions for two different electric currents. This delta of the magnetic force is important for the shape of the valve´s Q-I curve.

Number 2 (dark blue) limits the force at zero stroke and maximum current to a specific minimum. This constraint is used as an objective for the first optimization with an evolutionary algorithm.

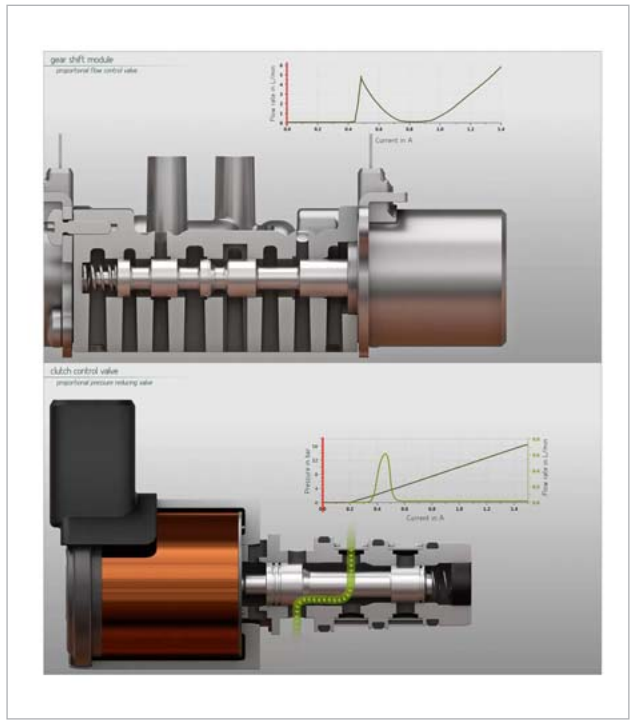

Fig.1: Hilite gearshift valve (top) and clutch control valve (bottom) for DCTs

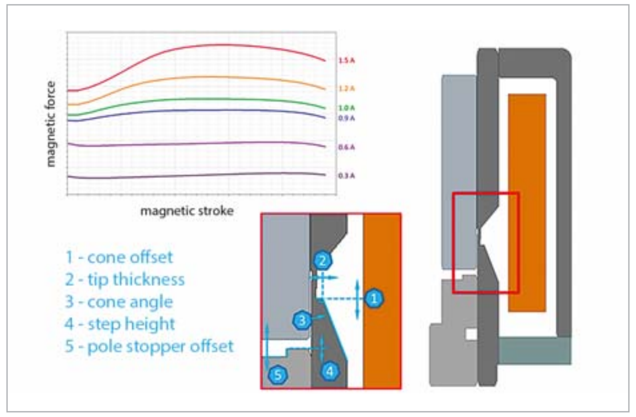

Fig. 2: Parameterized Maxwell model with force curve

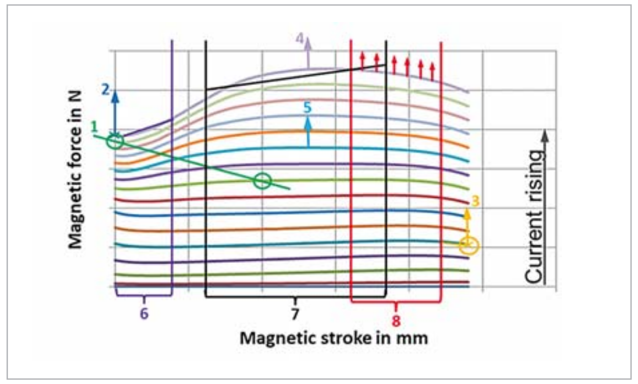

Fig. 3: Field of magnetic force over stroke with criteria for optimization

Number 3 (yellow) ensures a minimum amount of force at maximum stroke for low current. Furthermore, the slope is restricted as well.

Number 4 (light purple) sets a lower limit for the magnetic force at maximum current that effects all stroke positions. Thus, the magnetic force always keeps a minimum level.

Number 5 (light blue) works like number 4 but is valid for an intermediate current.

The Number 6 constraint (dark purple) limits the slope of the curve to a minimum in a specific region of small stroke positions. Number 7 (black) operates similar to constraint 6 but the region contains middle stroke positions.

Number 8 (red) is an objective and aims to maximize the magnetic force at large electric current in an area of large stroke.

Parametric system

The integration of the simulation program Maxwell into the optimization program optiSLang can be done in various ways. One way would be using the AEDT integration that is available in optiSLang since version 7.3. It is easy to create and performs very effectively. As the only problem so far, there is no comfortable way to work with signals.

The only way to optimize the characteristic curves of the magnetic force with Maxwell and optiSLang is to use a script-based integration. With this method, it is possible to let the constraints and objectives refer to the curves and picture them inside the optimization analysis. Moreover, with the amount of different stroke positions and currents that need to be computed for every design in order to create an accurate signal to work with, the script based integration method is almost as efficient as the integrated AEDT version.

In order to successfully build a working optiSLang system for Maxwell computations, one needs a working project (model, parameters, setup and results) at first. With the help of a Maxwell command, it is possible to extract the geometry parameters and the defined responses of the results in separate files (input, output). These files were used to set up the parametric system.

Figure 4 (see next page) shows the integrated Input, Solver and Output of the optiSLang system. The Maxwell files were implemented with a common text based solver, for example ANSYS Classic (Text Input – Batch Solver – ETK). The input node detects the input parameters. In the ETK node, one can define the force curves as signals and the batch solver activates the solver script to run Maxwell with different designs.

For every design five currents with up to 14 stroke positions per current are calculated, which sums up to 28 calculations for each design. The handling of these different computations are done with "Optimetrics" in Maxwell, which can be used with the script connection.

Figure 5 (see next page) shows the three most important parts of Maxwell, highlighted in blue frames. The model area "MX2D (a)" contains the variable geometry param-

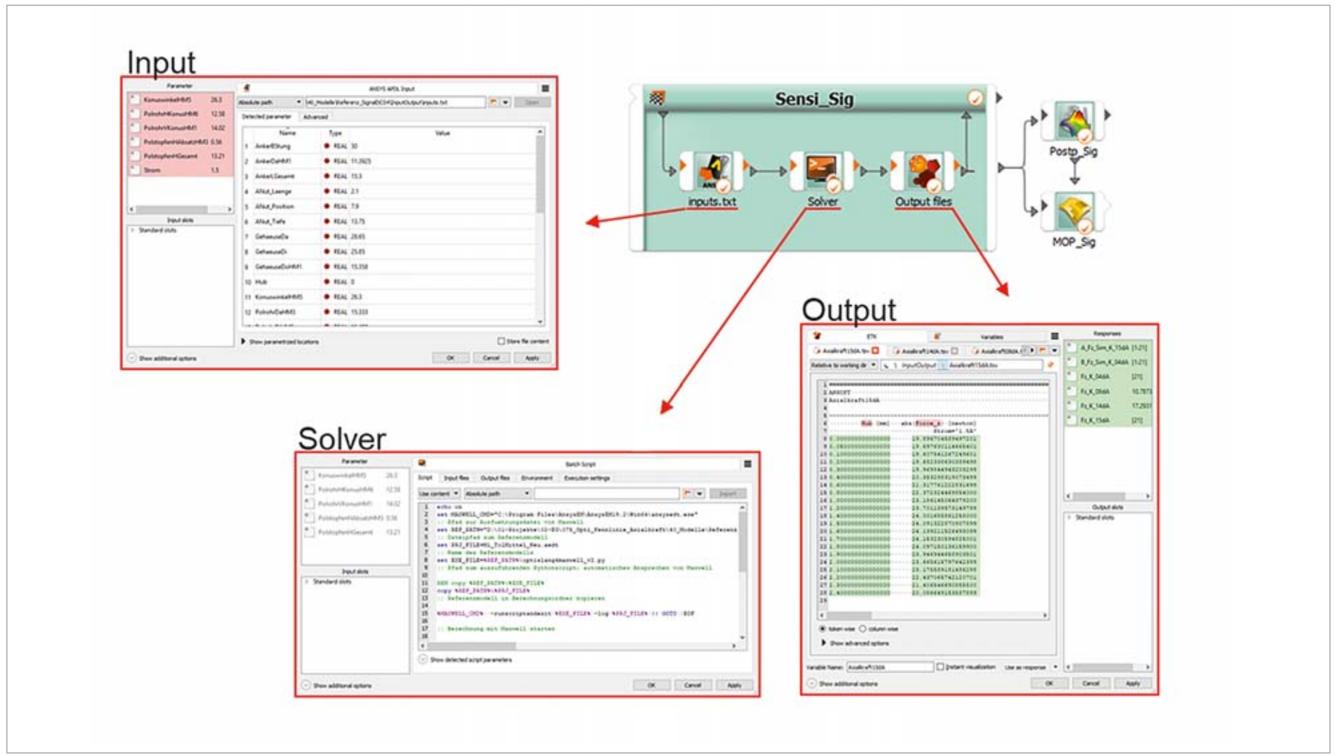

Fig.4: optiSLang System with Maxwell integration

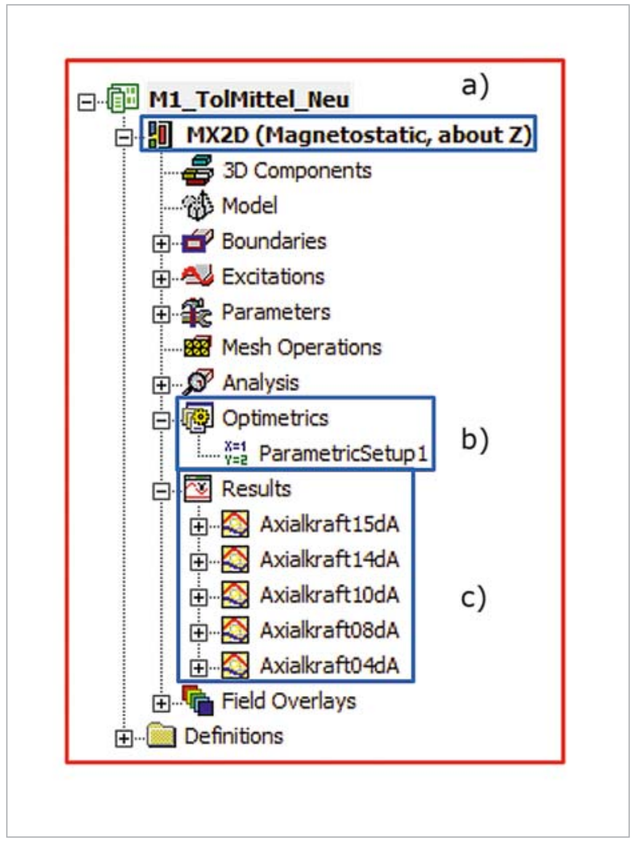

Fig. 5: Computation order in Maxwell with optiSLang; a) Input parameter creating geometry, b) Setup of variations, c) Definition of characteristic curves for output extraction

eters that optiSLang changes and imports into the Maxwell file for calculation. In "Optimetrics (b)", the different variations of stroke and current are listed and set up for computation. The pre-defined characteristic curves for the output extraction to optiSLang are saved in "Results (c)".

Computations

The integration of Maxwell into a parametric system in optiSLang helps to find optimal designs for actuator valves. The search for the best design includes a sensitivity analysis that identifies the important parameters and their mutual interplay. The information collected in the sensitivity analysis makes it possible to use the MOP- and Maxwell-Solver effectively in the optimization. The result of the optimization is implemented in system simulation models to obtain information about the performance of the valves.

Optimization

In the following Figure 6 one can see the CoP-Matrix as a result of the sensitivity analysis using the "Metamodel of Optimal Prognosis" (MOP). Here, the five geometry parameters are listed in the first row. The columns below express the influence on the change of the magnetic force at certain positions. The first and second column show these positions, which are combinations of current and magnetic stroke that define 28 output parameters. All strokes of every electric current combined results in a magnetic force curve that is different for each design. The different parameters have different influences for different currents and strokes. The higher the percentage the higher the influence for the calculated variation. The parameter "Total" at the end of the matrix tells the overall quality of the meta-model (100% means no error). The first three parameters "cone offset", "tip thickness" and "cone angle" have a large influence on the variation of the axial magnetic force at certain stroke positions. "step height" only has an influence on the force at small strokes and "pole stopper offset" has small influence overall.

With all the informations from the sensitivity analysis about force, stroke and current stored in the MOP, a usage in the optimization can lead to good and fast results. So, for the optimization of the magnetic force curves, Maxwell as well as the MOP was used as a solver.

The first optimization was done with the evolutionary algorithm (EA). It resulted in a pareto front which is shown in Figure 7 as a red line. As already mentioned in Chapter "criteria for optimization", the objectives of the EA were maximization of the force at zero stroke (2) and maximizing the force at high stroke (8). The results show the possible variation of the curve, which were used as start designs for the stricter single objective optimization with the adaptive response surface method (ARSM).

During the single objective optimization, two designs with different constraint values showed very good results. The history of these designs "ARSM21" and "ARSM51" is shown in Figure 8.

Figure 9 (see next page) shows the characteristic curve of the magnetic force over the magnetic stroke for 0.4 A, 1.0 A and 1.5 A. The curve of the reference design and the first EA are plotted with dashed lines. The optimization result "ARSM21" is depicted in blue and "ARSM51" in red. Due to the successful optimizations and the proper settings and definitions of the relevant criteria, all optimized designs got improved curves when compared to the base model (Reference). The design "ARSM21" can score with the largest force which occurs at 1.5 mm stroke. The design "ARSM51" however has a long smooth slope until the maximum, which is at 1.7 mm stroke.

System simulation

Both optimized designs "ARSM21" and "ARSM51" exhibit individual qualities and thusly are used in a system simulation that evaluates the valves behavior.

Current	Magnet. stroke	VersatzKonus	Spitzendicke	Konuswinkel	Polstopfen Versatz	HoeheAbsatz	Total
0.4 A	2.4 mm	100.00%	0.45%	0.14%	0.00%	0.01%	100.0%
0.4 A	2.2 mm	99.99%	1.94%	0.49%	0.00%	0.02%	100.0%
1.0 A	2.4 mm	86.26%	15.31%	1.29%	0.00%	0.04%	100.0%
1.0 A	2.2 mm	70.49%	26.34%	3.67%	0.00%	0.01%	100.0%
1.0 A	2.0 mm	40.24%	50.62%	10.64%	0.00%	0.03%	100.0%
1.0 A	1.8 mm	12.22%	69.97%	20.55%	0.06%	0.00%	100.0%
1.0 A	1.6 mm	11.74%	60.90%	30.62%	0.12%	0.29%	100.0%
1.0 A	1.4 mm	23.71%	41.12%	37.79%	0.11%	0.61%	100.0%
1.0 A	1.0 mm	51.73%	8.06%	43.94%	0.76%	3.12%	100.0%
1.0 A	0.6 mm	67.03%	21.49%	6.21%	2.36%	9.40%	100.0%
1.0 A	0.2 mm	44.47%	32.67%	7.48%	1.34%	15.33%	100.0%
1.0 A	0.0 mm	36.49%	27.47%	11.46%	0.89%	26.87%	100.0%
1.5 A	2.4 mm	73.01%	22.96%	4.04%	0.00%	0.00%	100.0%
1.5 A	2.2 mm	61.63%	31.42%	8.30%	0.00%	0.05%	100.0%
1.5 A	2.0 mm	35.29%	48.19%	18.63%	0.00%	0.11%	100.0%
1.5 A	1.8 mm	10.33%	58.37%	31.86%	0.08%	0.22%	100.0%
1.5 A	1.6 mm	11.60%	47.91%	44.21%	0.32%	0.66%	100.0%
1.5 A	1.4 mm	26.56%	27.84%	46.23%	0.94%	1.59%	100.0%
1.5 A	1.2 mm	49.63%	10.10%	40.83%	1.89%	3.08%	100.0%
1.5 A	1.0 mm	71.05%	5.55%	22.08%	3.50%	5.09%	100.0%
1.5 A	0.8 mm	75.19%	15.18%	5.93%	3.72%	5.59%	100.0%
1.5 A	0.6 mm	65.82%	27.59%	1.99%	3.06%	6.31%	100.0%
1.5 A	0.4 mm	56.34%	32.05%	4.85%	2.08%	7.36%	100.0%
1.5 A	0.2 mm	46.74%	33.67%	10.13%	1.34%	10.16%	100.0%
1.5 A	0.1 mm	42.93%	32.45%	12.70%	1.06%	13.84%	100.0%
1.5 A	0.0 mm	37.11%	29.25%	13.53%	0.89%	19.71%	100.0%
0.8 A	1.0 mm	47.14%	11.99%	45.18%	0.51%	2.11%	100.0%
1.4 A	0.0 mm	37.45%	28.89%	13.87%	1.02%	20.84%	100.0%

Fig. 6: Coefficient of Prognosis of the force in different positions for the input parameters, for different positions of the input parameters see also Fig. 2

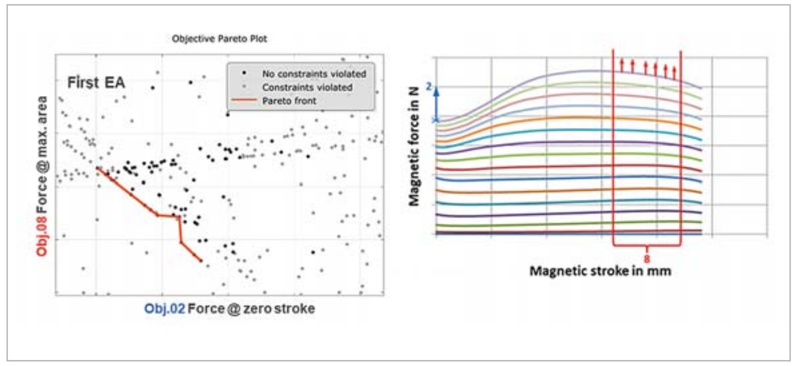

Fig. 7: Pareto front of the evolutionary algorithm (left) and its two objectives (right)

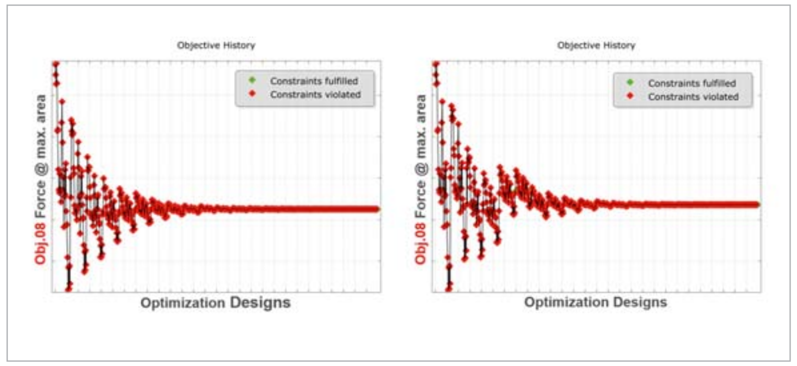

Fig. 8: History of the optimizations with adaptive response surface method

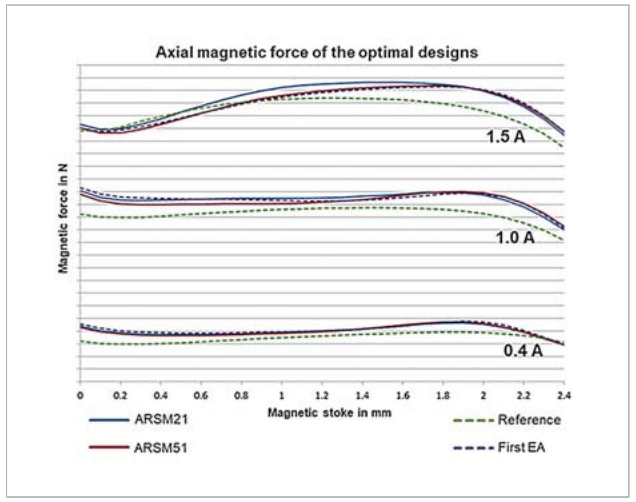

Fig. 9: Magnetic force with different currents and optimization Designs

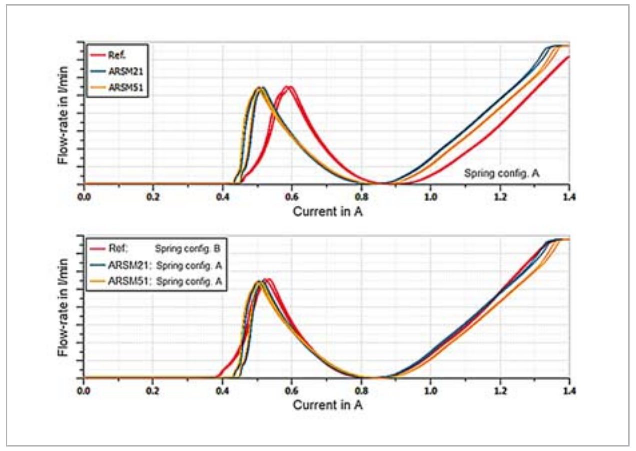

Figure 10: Flow rate over current for optimized designs ARSM21 & 51 with system simulation of gearshift valve

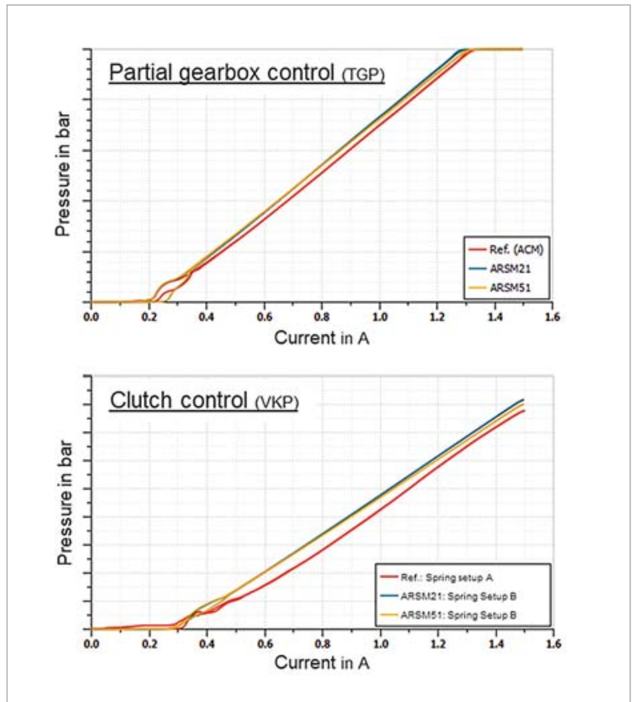

Figure 11: Pressure over current of TGP and VKP with system simulation

The difference between "ARSM21" and "ARSM51" mainly occurs between 0.9 A and 1.3 A. The appropriate characteristic curve of the gearshift valve shows Figure 10 (see next page) with different spring configurations in the two pictures. Both valves with optimized magnets reach the first peak in the Q-I curve earlier than the reference design and continue decreasing slower towards the minimum. In the second peak with currents larger than 0.9 A, "ARSM21" equals the base model and "ARSM51" remains below the other curves.

Both new actuator designs allow the usage in different valve types. The optimized designs achieve slightly better results than the reference in the system simulation of the TGP that is pictured on the top side in Figure 11. In the VKP on the bottom, the optimized designs have straight curves and fewer oscillations, something that is not visible in the reference design.

Conclusion

With the possibility of optiSLang and Maxwell working together even complex issues can be solved. The example shows that the valve can be optimally adjusted to its designated function and with further developments, even faster and better results are possible.

Authors //
Christian Hugel (Hilite Germany GmbH)

References

www.dynardo.de: Change Log ANSYS optiSLang. URL https://www.dynardo.de/software/optislang/changelog-ansys-optislang.html, 2019

SCHUMACHER, A.: Optimierung mechanischer Strukturen – Grundlagen und industrielle Anwendungen, Springer-Verlag, 2013

STOCKMEIER, M.: Driving efficient design variation studies using ANSYS Electronics Desktop and optiSLang, Dynardo GmbH, December 2019

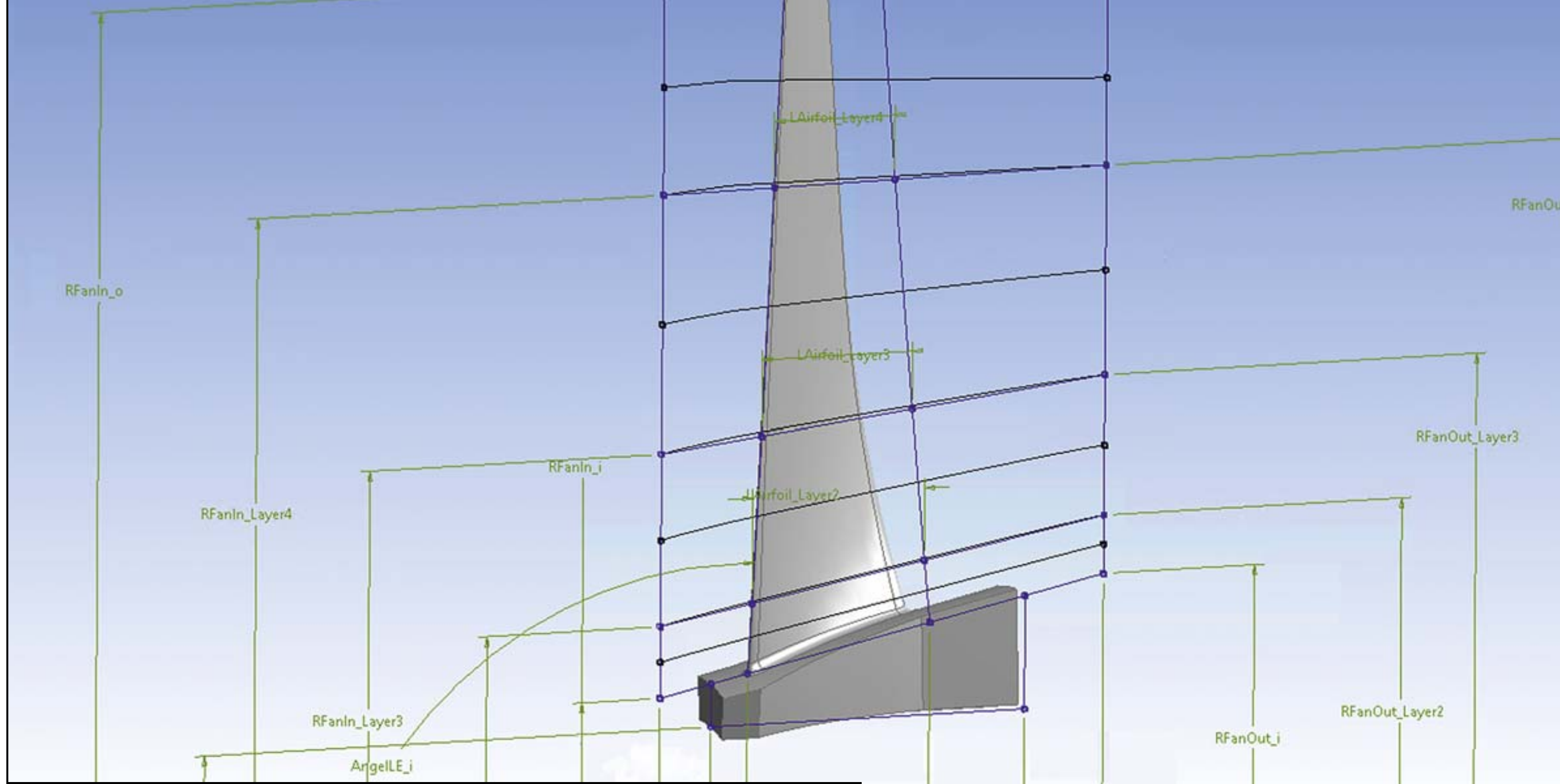

CASE STUDY // TURBO MACHINERY

MULTIDISCIPLINARY OPTIMIZATION OF A CIVIL TURBOFAN JET ENGINE

Using ANSYS and optiSLang, the design of a turbofan jet engine was improved regarding polytrophic efficiency and mechanical stresses in the fillet and the blade of the fan.

Motivation

This article contributes to the field of multidisciplinary optimization of turbomachines. Here, the focus is on the fan of a civil turbofan jet engine with a high bypass ratio. Conceptual design methods were used to determine the aerodynamic characteristics. For more detailed analyses, a numerical 3D-CFD and 3D-FEA model was set up for the take-off conditions of the fan (close to stall). Based on these results, the design was improved iteratively and manually regarding polytrophic efficiency and mechanical stresses in the fillet and the blade of the fan.

Recent developments in the product development process go beyond successive simulation and analysis of individual design solutions and results. Computational approaches for sensitivity analysis, optimization and robustness evaluation integrate a variety of simulation results to foster system understanding for engineering design.

The automation of the process and the numerical effort are challenges for such methods. The automated workflow is implemented in ANSYS optiSLang and ANSYS Workbench that includes a stable parametrized geometry model, automated meshing, CFD runs and post processing.

Due to the numerical demanding CFD simulations, an efficient method is necessary to enable parametric studies and optimizations with an acceptable numerical effort. To satisfy these requirements, the workflow is used to run a sensitivity analysis first in order to calculate meta-models for all relevant result quantities. With the help of the meta-models, a fast pre-optimization by using different objectives was possible. By using only the important parameters indicated by the sensitivity analyses, an efficient optimization algorithm could be chosen in order to run a final direct optimization with the numerical model.

Civil turbofan jet engine: conceptual design method and numerical CFD and FEA model

First, conceptual design methods were used to determine the aerodynamic characteristics. With the help of the software GasTurb, the main dimensions of the fan could be calculated based on the requirements of the engine (e.g. pressure ratio Π, Bypass ratio). Afterwards, the blade geometry (e.g. camber line, blade thickness) and blade angles are calculated as well as the inlet geometry is designed.

A jet engine operates at a great variety of different operating conditions. Depending on the desired travel Mach number, the spool speed and the mass flow rate change. Since the highest mass flow rates occur during the take-off (close to stall), these flight and thermodynamic conditions have been used in the design process.

For detailed analyses, a numerical 3D-CFD and 3D-FEA model was set up. For that, the parametric geometry was designed with the ANSYS BladeModeler. Global parameters for describing the main dimensions of the fan were kept constant, while 25 parameters could be used to define the shape of the blade itself. This included 5 parameters to describe the meridional plane, 8 parameters for the blade angles, 8 parameters describe the blade thickness and one parameter for the number of blades, blade lean circumferential and fillet radius.

The appropriate definition of parameter dependencies and bounds are essential in turbomachinery optimization. Therefore, usually the parametrization is not suitable after the first attempt. Consequently, for ensuring a stable geometry generation a Design of Experiments only for the geometries itself is useful. By statistical evaluation of failed designs, additional dependencies can be implemented, existing dependencies adapted and parameter bounds adjusted.

Exemplary for this parametrization is the meridional plane and the blade angles, which are explained in the following in more detail. Five airfoils at different span locations define the blade. Each airfoil has a length that is parametrized but not all are allowed to change within the Design of Experiments. Only the length at hub, shroud and the layer in the middle are adopted. The other lengths are adjusted accordingly. The leading-edge blade angles of the airfoils are are a second example, which varied independently at hub and shroud within the Design of Experiments. The other leading-edge blade angles are parameterized, but in order to ensure useful designs only hub and shroud are varied independently. The three angles at the layers in between are varied as parameters, but only in percentage within the current values of hub and shroud.

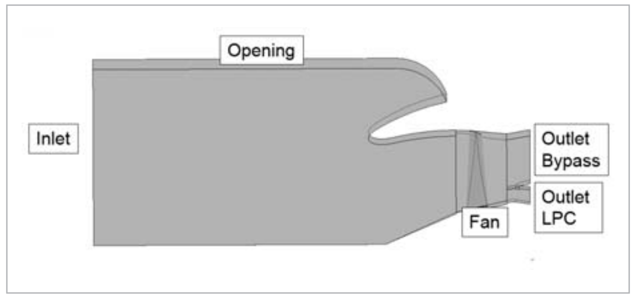

Fig. 1: CFD boundary conditions

The boundary conditions of the steady-state analyses of a periodic segment are shown in Figure 1. At the inlet, flight speed and ambient temperature for the take-off conditions are defined. The outlet is split in the bypass with static pressure and the LPC (low pressure compressor). At the opening, the ambient pressure is set. The meshing for the unchanged parts was conducted in ICEM. TurboGrid was used for the automated meshing of the fan domain. In CFD Post the output parameters like Π (pressure ratio) and polytrophic efficiency are defined.

Afterwards, a simplified FEA in ANSYS Mechanical is added to avoid implausible geometries from the structural mechanics point of view within the optimization process. In order to accomplish a reasonable numerical effort, a solid body is modeled instead of using a skeleton coated with CFK. Moreover, the deformation and the stresses in the blade and the fillet are of prime interest, the connection between the blade root and the hub disc is neglected in this analysis. The imported loads for the fan are the pressure on the blade coming from the previous CFD calculation and the rotational velocity. The cylindrical support and the cyclic symmetry are the boundary conditions.

Based on these results, the design was improved iteratively and manually regarding polytrophic efficiency, Π (pressure ratio), total deformation and mechanical stresses in the fillet and the blade of the fan. Figure 2 depicts the flow around the airfoil at different operating points and span locations. It can be proven that the flow meets the blade at the right angle.

Results of the sensitivity analysis

As a framework for geometry model, meshing and solver runs (including the mapping of the pressure field to the FEA) the ANSYS Workbench is used. This model was integrated in ANSYS optiSLang for an optimization workflow.

In order to ensure that the geometry and mesh can be generated and the solver covers the whole design space properly, a sensitivity analysis was carried out in ANSYS optiSLang. The design space was defined by the lower and upper bounds of the parameters. A sensitivity analysis scans the space and evaluates the variance of the inputs (e.g. geometry parameters) in relation to the output parameters (e.g. Π pressure ratio). For this purpose, the Design of Experiment is generated by an optimized Latin Hypercube Sampling [1]. For each sample, the output parameters are evaluated by the solver. With help of the Metamodel of Optimal Prognosis (MOP) approach [2] an optimal mathematical surrogate model (meta-model) was generated for each scalar response value.

In total, 188 of 200 designs for the sensitivity analysis are calculated successfully. In order to ensure the evaluation of the convergence, for each design relevant physical quantities are extracted. Consequently, 149 designs could be indicated as converged and after neglection of outliers 138 designs are used to generate the MOP. Figure 3 shows the MOP for the polytropic efficiency with a CoP of 78% which used 18 input parameters (that have a significant influence on the response) to build the meta-model. The leading edge radius at the hub (LERadius_i) and the length of the airfoil at layer 3 (LAirfoil_Layer3) have the highest influence for the given parametrization. It has to be noted that the importance of parameters will change by using different parameter variation windows. In this example, the design was manually pre-optimized and therefore the variation window for the blade angles was set rather

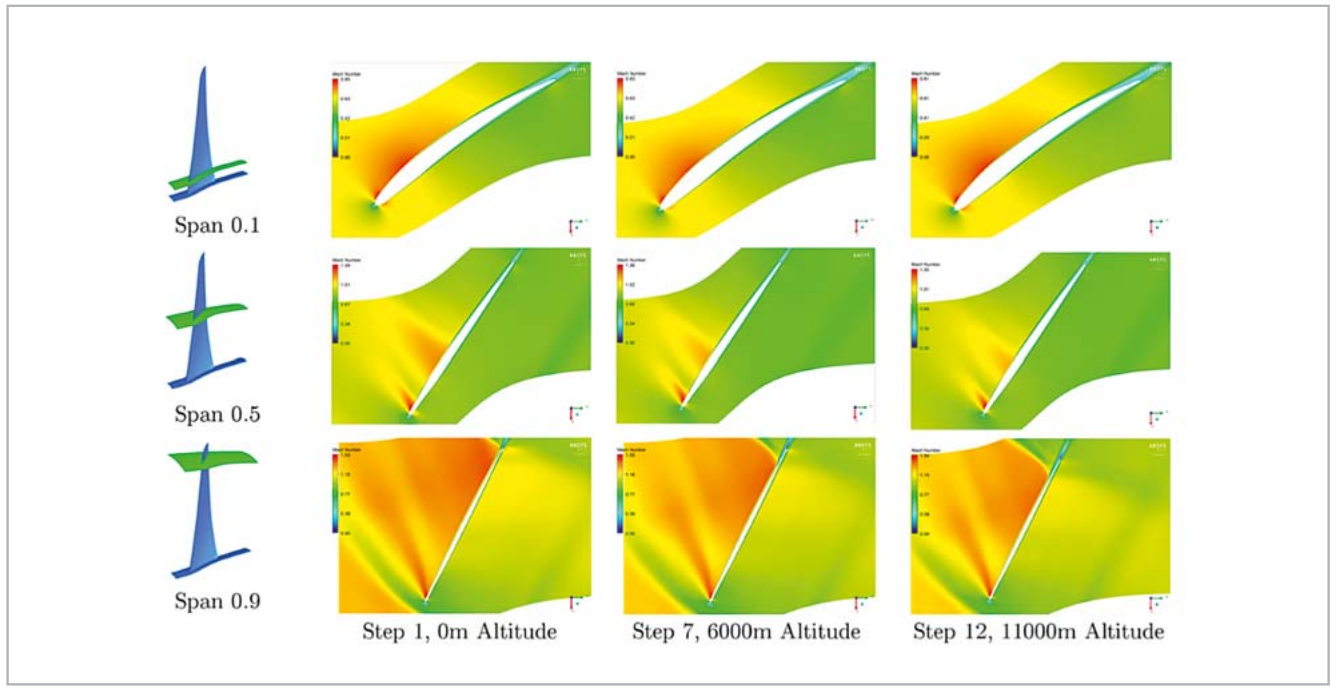

Fig. 2: Flow around the airfoil at different span locations and operating points

narrow. Thus, they have an influence (e.g. ReaktionRatio_o or betaIn_o), but not a dominating one.

Optional subsequent strategies that derive from the analysis are: a) increasing of the number of designs of the sensitivity in order to get a more accurate meta-models with a higher CoP value (this is very likely since the number of important variables is high and only 200 designs have been evaluated), b) to conduct a second sensitivity analysis in a narrower design space defined by the parameters of the best designs of the first sensitivity or c) to do a pre-optimization on the given MOP and use this improved design for a direct optimization. Due to the numerical demanding CFD simulations, the third strategy was chosen.

Optimization

The main objective was the increase of the polytrophic efficiency. Due to the requirements of the jet engine itself, the pressure ratio Π should be above 1,2. Moreover, the unaveraged stresses in the blade and the fillet should not exceed 1000 N/mm² and due to the tip gap of 6 mm the radial deformation of the blade must be under that value.

The meta-models are used for pre-optimization, since the forecast quality of the efficiency is almost 80%. Different formulations of objectives and constraints can be easily tested, adapted and fast evaluated. In the left Figure 4 the convergence of the Evolutionary Algorithm by using the MOP and the improvement of the objective is shown. This calculation of more than 3500 design evaluations is done in minutes, while one CFD run takes hours. As shown, the algorithm starts in an area with lots of constraints violations (red) and moves in a subspace with less constraint violations (green) in the local search at the end. The best design

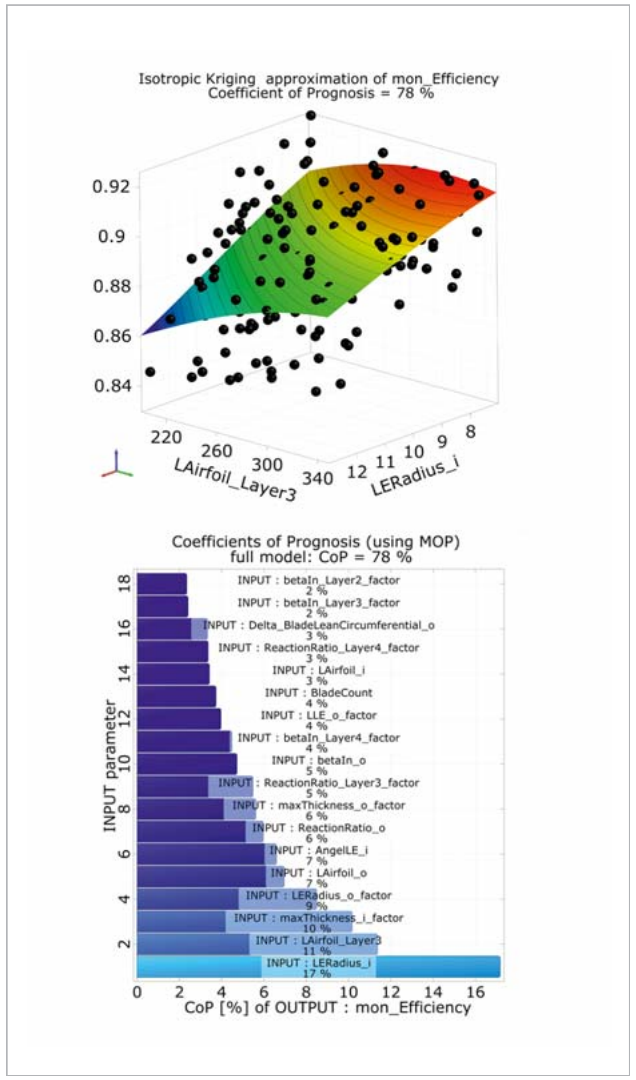

Fig. 3: Meta-model (top) and important parameters (bottom)

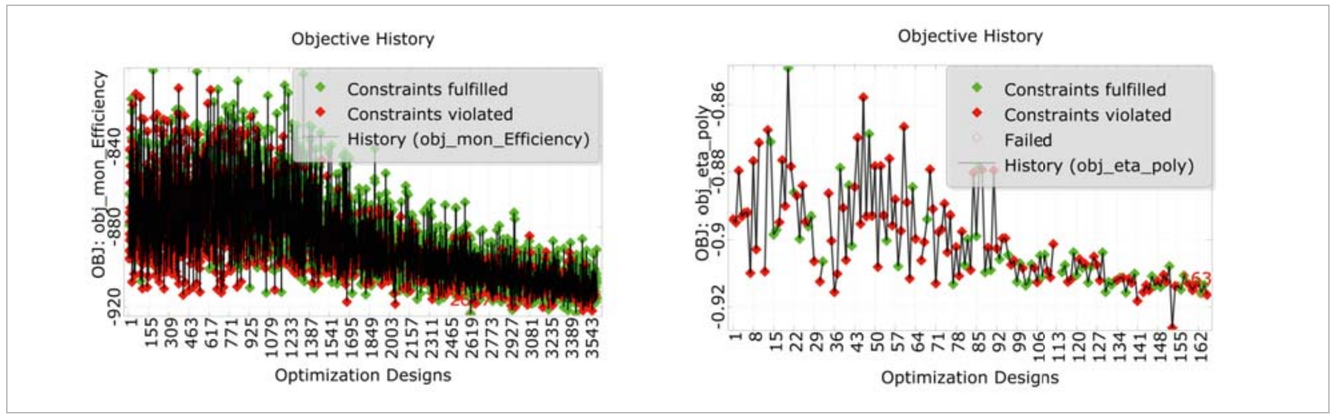

Fig. 4: Convergence history of Evolutionary Algorithms in the MOP (left) and direct optimization using an ARSM algorithm (right)

	Manual optimized	Best Sensitivity	Opt. on MOP (validated)	ARSM (Direct optimization)
Polytrophic Efficiency [%]	90,94	92,01	92,63	92,83

Fig. 5: Polytrophic efficiency in optimization process

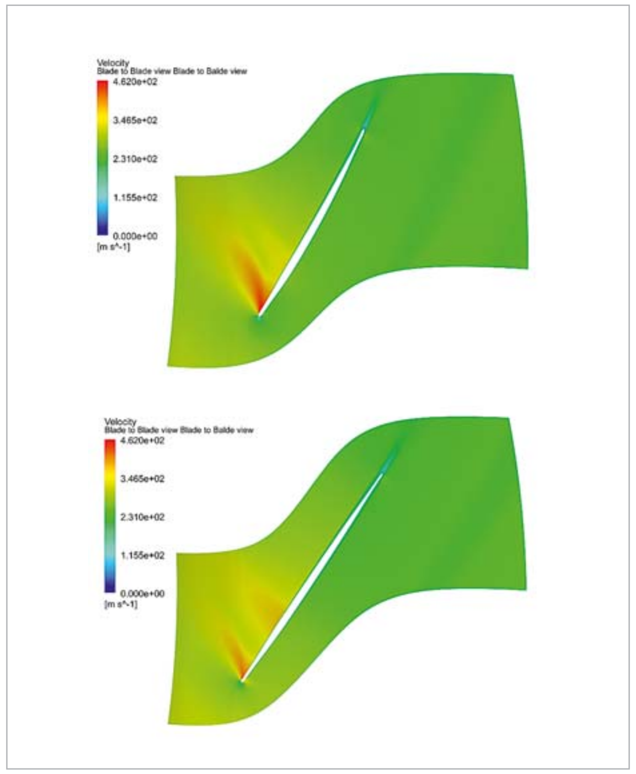

Fig. 6: Flow around an airfoil at span 0,5: manual optimized (top) and best design after optimization (bottom)

has improved the polytrophic efficiency by 1,7% from 90,9% to 92,6% (Fig. 5). After finishing the MOP-based optimization, the best design candidates need to be validated with CFD/FEM runs.

Based on this pre-optimized design an Adaptive Response Surface Method (ARSM) was applied in a second step using CFD/FEM design evaluations. The start design was the best design from the pre-optimization and the algorithm used the reduced number of parameters, which were indicated as important in the sensitivity analyses. Within a few iterations a further improvement was possible to an efficiency of 92,8%, which is an increase of 1,9% compared to the manual optimized design. Again, all the mechanical constraints were fulfilled and also the needed pressure ratio (Π) was reached. In Fig. 6 the velocity field is shown an 0,5 span. In both designs, the flow meets the blade at the right angle and the maximum velocity is lightly reduced in the best design of the optimization.

Summary

A civil turbofan jet engine with a high bypass ratio was manually optimized by conceptual design methods and with the help of a 3D-CFD and 3D-FEA model. This design was used as a basis for an optimization procedure with the objective to increase the polytrophic efficiency while the pressure ratio (Π), mechanical stresses in the fillet and radial deformation had to fulfill given constraints. By conducting a sensitivity analysis, pre-optimization on the metamodel and direct optimization, the polytrophic efficiency could be increased by 1,9% from 90,9% to 92,8% while the given constraints were still fulfilled.

A possible next step is to add desired altitudes for the jet engine, which means for the optimization to include multiple operating points in one design evaluation.

Authors // M. Wagner (Dynardo GmbH), Prof. Dr.-Ing. M. Geller (FH Dortmund), J. Einzinger (ANSYS Germany GmbH)

References
[1] Iman, R. L. & W. J. Conover "A distribution-free approach to inducing rank correlation among input variables" Communications in Statistics - Simulation and Computation 11, 311-334, 1982

[2] Most, T. & Will, J., "Sensitivity analysis using the Metamodel of Optimal Prognosis", Proceedings of the Weimar Optimization and Stochastic Days 8.0, 2011

CASE STUDY // AUTOMOTIVE ENGINEERING

SAFETY ASSESSMENT OF AUTOMATED DRIVER ASSISTANCE SYSTEMS

Statistical methods combined with Software-in-the-Loop (SiL) simulation help to analyse the reliability of Advanced Driver Assistance Systems (ADAS).

Scenario-based driving simulation

The validation of Advanced Driver Assistance Systems is performed with a scenario based simulation. Simulation in this context means that the control device, on which the ADAS are running, is present as a simulation tool, running the real ECU code and thus software-in-the-loop simulations are performed. All inputs for the simulated controller are generated by a simulation environment. These include sensors, vehicle data as well as data from other ECU's installed in the vehicle. In order to generate plausible input data, a virtual environment is simulated in which the system vehicle moves and other road users (objects) are detected by sensor models. Thus, the virtual world is processed and captured, and control quantities calculated therefrom are delivered back to the vehicle model.

For the scenario-based approach, a number of logical scenarios describable by parameters are defined [Menzel]. The scenarios are derived from the system requirements, from the research project PEGASUS (Joint project to develop new methods for validating and testing ADAS) as well as observations from the field. A logical scenario is typically a specific traffic situation. For instance, a cut in maneuver of other objects or a jam end situation on a highway as shown in Figure 1 (see next page). To describe such a logical scenario the 6-Layer model can be used [Bock]. For demonstration purposes, only the road layer (1) and the moving objects layer (4) are used for the description. With the help of the corresponding parameters, these logical scenarios can be varied in their characteristics. Hence it is possible to vary speeds of the vehicles, distances from objects or the dynamics of lane change maneuvers. These so-called specific scenarios resulting from different parameter combinations are simulated and the system reaction of the ADS is evaluated. This is done through evaluation criteria that reflect the criticality of a specific scenario. For example, the Time-To-Collision (TTC) or the distance between two vehicles can be used as evaluation criteria.

The intention of the methodology described in the following is to determine the probability of failure for each logical traffic scenario. Therefore, the parameter space is searched with an intelligent algorithm to determine the probability that a critical situation or even an accident can occur. The probability distributions of the input parameters as well as the probability of occurrence of the respective scenario are determined based on real measured data and by using the PEGASUS database [Pütz].

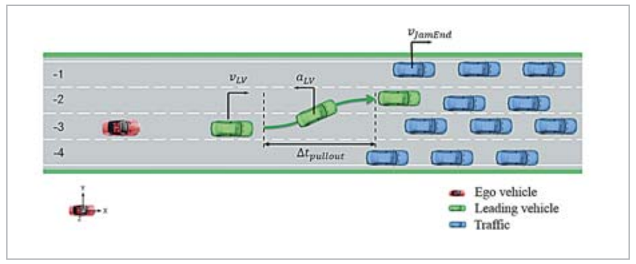

Fig. 1: Jam end traffic scenario on the highway. By altering the input parameters this logical scenario can be varied in its characteristics.

Stochastic Analysis

Satisfying design requirements will necessitate ensuring that the scatter of all important responses by fluctuating geometrical, material or environmental variability lies within acceptable design limits. With the help of the robustness analysis this scatter can be estimated. Within this framework, the scatter of a response may be described by its mean value and standard deviation or its safety margin with respect to a specified failure limit. The safety margin can be variance-based (specifying a margin between failure and the mean value) or probability-based (using the probability that the failure limit is exceeded). In Figure 2 this is shown in principle.

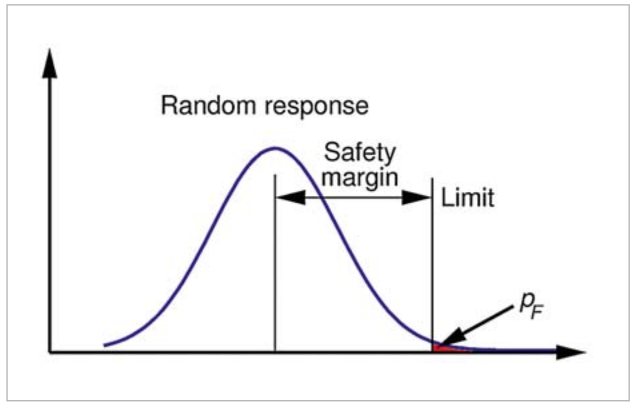

Fig.2: Scatter of a fluctuating response with safety margin (distance between mean and the failure limit) and the corresponding probability of failure p_F.

Within the reliability method the probability of reaching a failure limit is obtained by an integration of the probability density of the uncertainties in the failure domain. One well-known method is the plain Monte Carlo Simulation [Rubinstein], which can be applied independently of the model non-linearity and the number of input parameters. This method is very robust and can detect several failure regions with highly non-linear dependencies. Unfortunately, it requires an extremely large number of model evaluations to proof rare events. Therefore, more advanced sampling strategies have been developed like Importance Sampling, where the sampling density is adapted in order to cover the failure domain sufficiently and to obtain more accurate probability estimates with much less solver calls. Other methods like the First or Second Order Reliability Method (FORM & SORM) are still more efficient than the sampling methods by approximating the boundary between the safe and the failure domain, the so-called limit state. In contrast to a global low order approximation of the whole response, the approximation of the limit state around the most probable failure point (MPP) is much more accurate. A good overview of these "classical" methods is given in [Bucher].

In our study we have investigated several methods. One reliable and robust method for our application is the Adaptive Importance Sampling strategy [Bucher]. In this approach an importance sampling density is obtained by iterative adjustment of a modified sampling density.

This method becomes inefficient with increasing number of random variables due to the less accurate estimates of the density statistics. Therefore, it is recommended to apply this method for problems with up to twenty random variables. Furthermore, it can analyze only one dominant failure region. In our studies, where discrete distribution types have been used together with continuous random variables, we observed an additional numerical effort to obtain a similar accuracy of the failure probability estimates as in pure continuous problems. This is caused in artificial discontinuities of the limit state function in the standard normal space as shown in Figure 3. Even for continuous limit state functions such discontinuities occur due to the discrete distributions. This phenomenon causes multiple most probable failure points, which makes the normal sampling density less efficient.

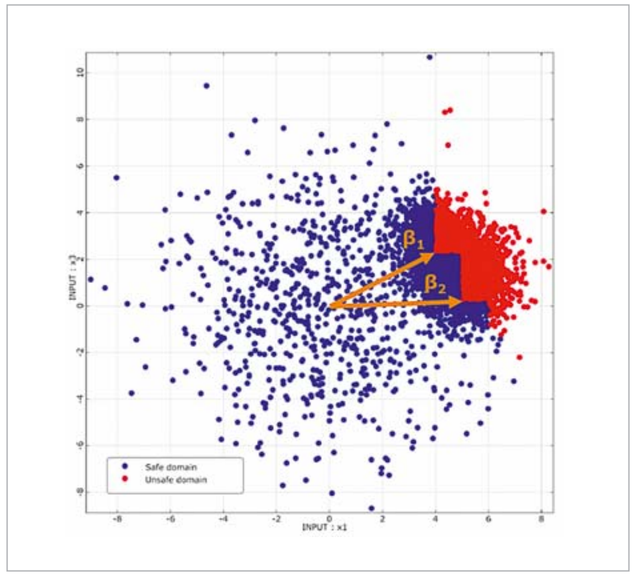

Fig. 3: Adaptive Importance Sampling for a linear limit state function considering discrete random variables, samples in the standard Gaussian space.

On order to overcome the limitation of one dominant failure region we extended the Importance Sampling using Design Points (ISPUD) by a multi-modal density according to [Geyer]. The modified sampling density may consist of an arbitrary number of individual sampling densities with different center points and unit covariance in the Gaussian space. In Figure 4 the sampling is shown for four individual failure regions.

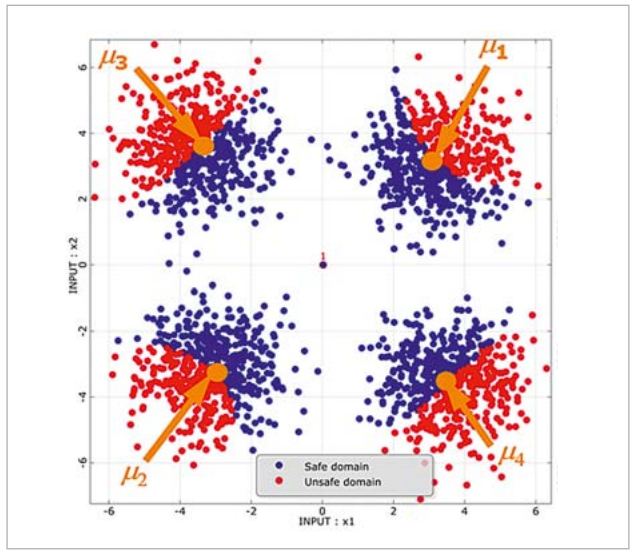

Fig. 4: Importance Sampling using Design Points generated by a multi-modal sampling density which consists of several standard normal densities.

In order to detect the individual failure regions with sufficient confidence, we extended the multiple FORM algorithm [Kiureghian]: Based on given start points or an initial presampling similar to the first iteration of the Adaptive Importance Sampling approach, we perform a local optimization several times. With help of a local gradient-based optimizer the closest point, where the limit state turns from safe to unsafe and which has the smallest distance to the median point on the standard normal space, is detected. Since the start points are selected using a density criterion by considering the previous optimization runs, we can assure that with a given number of local optimization runs, the important failure regions can be found. In case that some of the input parameters are modeled with a discrete distribution type, the local optimization is performed only in the reduced continuous subspace, but different combinations of the discrete values are investigated.

After the most important failure regions have been detected, the corresponding most probable failure points are used as centers for the sampling densities in the multi-modal ISPUD approach. Since the failure probability is not estimated by the beta-distance analogous FORM but by the more accurate Importance Sampling, even non-linear limit state functions can be accurately evaluated. Furthermore, the local optimizer needs not to be very accurate in the estimate of the local most probable failure points.

Application Example

In this example we investigate the jam end scenario where an ego vehicle including a lead vehicle drive to the end of a traffic jam on a highway. At a certain time, the lead vehicle will change the lane and the ego vehicle has to detect the last vehicle of the jam in order to perform an accident-free braking. In the simulation software the Time-To-Collision (TTC) is estimated w.r.t. the given input parameters. We consider this TTC as limit state and investigate several limits with the reliability algorithms. As input scatter we assume nine continuous scattering parameters as lead vehicle and jam end speed, pull out time, lead vehicle braking deceleration as well as a lane offsets of the traffic jam and the lead vehicle. The number of road lanes, the lead vehicle class and the pull out direction have been modeled with discrete random distributions.

In order to perform the analysis and verification more efficiently, in a first step a global meta-model was created based on 1000 samples. In order to obtain more samples and thus higher accuracy in the relevant regions a local adaptation strategy was used (Adaptive Metamodel of Optimal Prognosis, [Dynardo, Most]). Based on this fast meta-model we investigated the multimodal and Adaptive Sampling Importance Sampling in comparison to the brute-force Monte Carlo Simulation. In Figure 5 one subspace of the 12-dimensional meta-model is shown. As indicated in the figure, the lead vehicle speed and the jam end speed are most important in this scenario. Furthermore, the relation of the Time-To-Collision and the input parameters is almost monotonic. Thus, we would expect to obtain different failure regions mainly due to different combinations of the discrete parameters.

In Figure 6 (see next page) the convergence of the multiple FORM is shown for one specific failure limit. It can be

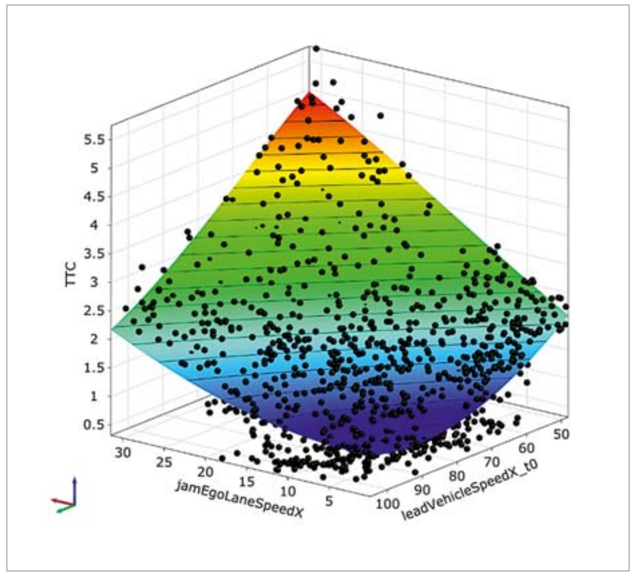

Fig. 5: Jam end scenario: adaptive meta-model used for the verification of the reliability algorithms

seen, that the optimizer converged to different reliability index values, which correspond to different most probable failure points. Altogether, 20 failure points have been detected which are used as sampling centers for the importance sampling.

	Number of samples	Failure probability	Coefficient of variation	Reliability index
Limit TTC = 1.0				
MCS	30.000	$1.61*10^{-2}$	4.5%	2.14
AS	8.000	$1.30*10^{-2}$	5.8%	2.22
ISPUD+FORM	2.000+6.400	$1.70*10^{-2}$	6.8%	2.12
Limit TTC = 0.5				
MCS	14.010.000	$2.86*10^{-5}$	5.0%	4.02
AS	16.000	$2.85*10^{-5}$	8.4%	4.05
ISPUD+FORM	4.000+4.500	$3.03*10^{-5}$	8.8%	4.01
Limit TTC = 0.4				
MCS	39.420.000	$2.54*10^{-6}$	10.0%	4.56
AS	16.000	$2.81*10^{-6}$	9.1%	4.54
ISPUD+FORM	7.000+5.500	$2.31*10^{-6}$	9.5%	4.58

Table 1: Estimated failure probabilities for different limit state limits using the global meta-model

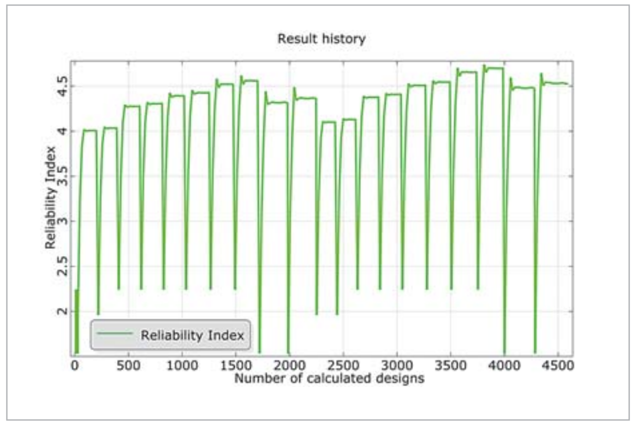

Fig. 6: Convergence of the multi FORM-search assuming a limit of 0.5s for the time-to-collision

In Table 1 the obtained estimates of the failure probability are given for the different limit values. The multi-modal and adaptive Importance Sampling strategy are compared to the results of the Monte Carlo Simulation. As indicated in the table, we could obtain a very excellent agreement of the results. As indicated, the multi-modal ISPUD is the most efficient algorithm, especially for small failure probabilities, which is the expected application field. In Figure 7 the importance sampling density is shown for the three most important parameters in the orginal parameter space.

Next, the multi-modal and adaptive Importance Sampling are applied using the traffic simulation software directly. The Monte Carlo Simulation could not be applied due to the large numerical effort. In Table 2 the results are compared. Again, the results of both methods agree very well, while the ISPUD approach needs less samples. Since the FORM method

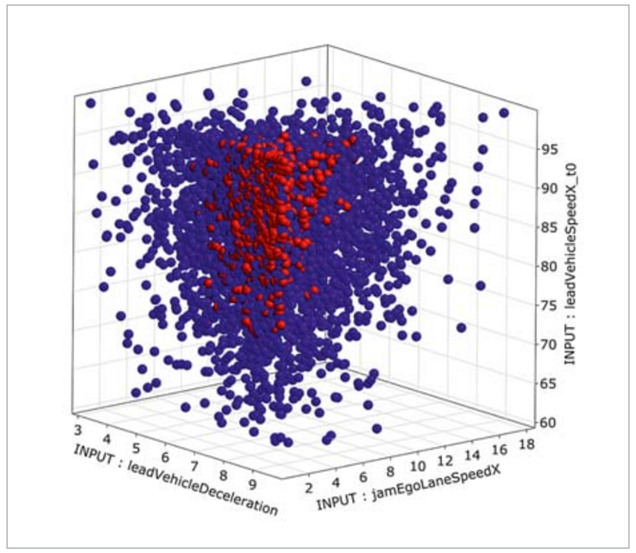

Fig. 7: Jam end scenario: joint multi-modal

is applied on the meta-model only, all together 1000 samples for the meta-model plus 5000 samples are needed. However, the estimates with the real solver indicate a much larger failure probability as estimated using the meta-model. Therefore, in our applications we always apply the ISPUD approach using the direct solver. If the most probable failure points are not estimated very accurately, we obtain still valid results since the ISPUD algorithms are running the sampling until a certain accuracy of the estimated failure probability is obtained.

Finally, we investigate the influence of the accuracy of obtained most probable failure points. For this purpose, we use the meta-model again by considering a failure limit of 0.5s for the time-to-collision. We initiate wrong failure points by

Limit TTC = 0.5	Number of samples	Failure probability	Coefficient of variation	Reliability index
MCS	Not possible	-	-	-
AS	22.000	5.30*10-3	9.2%	2.55
ISPUD+FORM	5.000 (+4.500 on meta-model)	4.40*10-3	20.1%	2.62

Table 2: Estimated failure probabilities for one limit state using the traffic simulation tool directly

Customer Story // Automotive Engineering

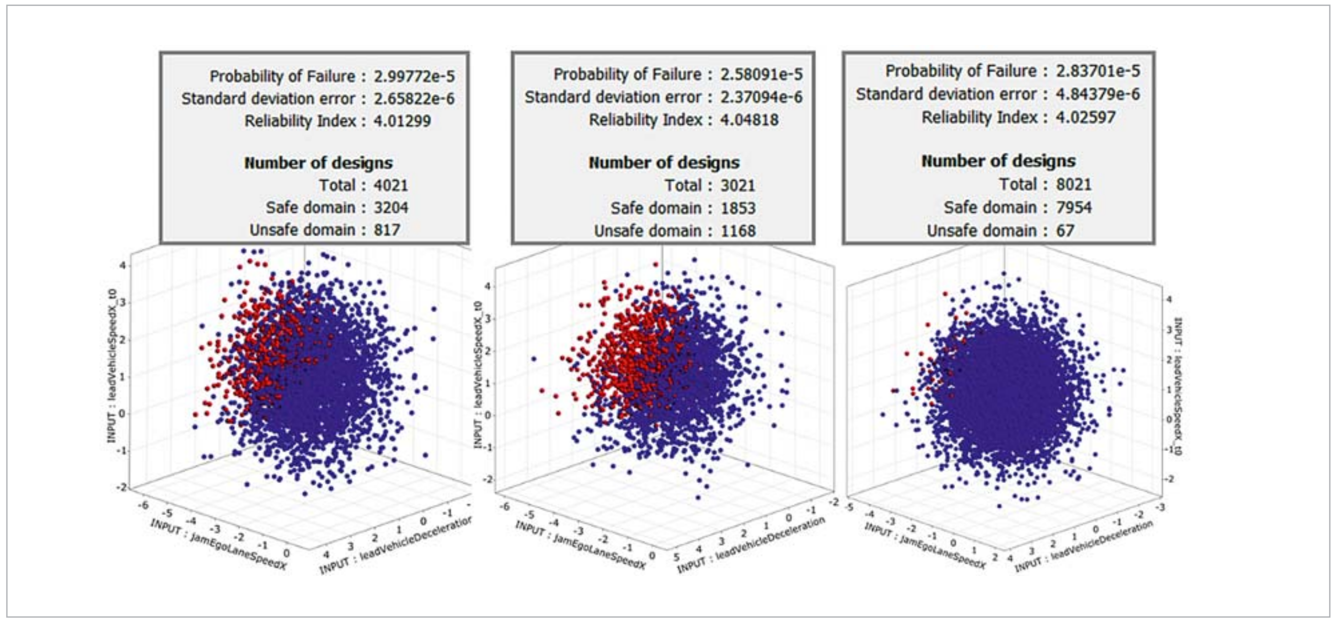

Fig. 8: Influence of the accuracy of the obtained most probable failure points using a limit of 0.5s on the meta-model: left – original results, middle – failure points are located in unsafe region, right – failure points are located in safe region

modifying the limit state in the FORM search while keeping the original one in the ISPUD sampling. In Figure 8 the results are illustrated. It can be seen, that if the density center points are shifted inside the failure regions, the number of unsafe samples increases which would increase the accuracy of the estimated failure probability. Therefore, less samples are necessary to obtain the required accuracy of 10%. In the other case, when the estimated failure points and thus the center points of the importance sampling densities are located too far in the safe region, the number of samples in the unsafe region decreases and thus the total number of required samples in ISPUD increases. Nevertheless, in all three cases the estimate of the failure probability was quite accurate.

Conclusion

In this paper we have presented an automatic approach for the reliability evaluation of specific traffic scenarios for the validation of Advanced Driver Assistance Systems. In this analysis the control device is represented as a simulation model using software-in-the-loop technology. Specific inputs of this simulated controller are modeled as random inputs in a stochastic analysis. Based on a definition of a failure criterion well known reliability algorithms could be applied. In our study we have used classical Monte Carlo Simulation only for verification due to its enormous numerical effort to proof small event probabilities. In order to reduce the number of necessary simulation runs, variance reduced importance sampling was applied. For this purpose, we used a multiple design point search approach to detect the important failure regions. Based on this result a multi-modal importance sampling density was automatically generated in order to quantify the contribution of each failure region to the overall failure probability. Based on a confident error estimate we could ensure, that the sampling loop was continued until a required accuracy of the probability estimate was obtained. The presented approach enables the automatic reliability proof of an Advanced Driver Assistance System for a specific scenario with minimum manual input. However, one very important point is the quantification of the input uncertainties of the investigated scenario. These assumptions strongly influence the finally estimated failure rate, therefore, attention should be paid in order to derive suitable assumptions about distribution type, scatter and event correlations from real world observations.

Authors //
Maximilian Rasch, Paul Tobe Ubben (Daimler AG)
Thomas Most, Veit Bayer, Roland Niemeier (Dynardo GmbH)

References

www.dynardo.de: Change Log ANSYS optiSLang. URL https://www.dynardo.de/
BOCK, J., KRAJEWSKI, R., ECKSTEIN, L., KLIMKE, J., SAUERBIER, J., AND ZLOCKI, A.: Data Basis for Scenario-Based Validation of HAD on Highways In: 27th Aachen Colloquium Automobile and Engine Technology. , 2018, 1389 – 1404

BUCHER, C: Computational Analysis of Randomness in Structural Mechanics., London, CRC Press, Taylor & Francis Group, 2009

BUCHER, C: Adaptive Sampling – an iterative fast Monte Carlo procedure., Structural Safety, 119-126, 1988

DER KIUREGHIAN A., T. DAKESSIAN: Adaptive Sampling – an iterative fast Monte Carlo procedure., Structural Safety, 119-126, 1988

DYNARDO GMBH: Methods for multi-disciplinary optimization and robustness analysis., optiSLang 7.3 documentation, 2019

GEYER, S., I. PAPAIOANNOU, D. STRAUB: Cross entropy-based importance sampling using Gaussian densities., Structural Safety, Volume 76: 15-27, 2019

MENZEL, T., BAGSCHIK, G., & MAURER, A. M.: Scenarios for Development, Test and Validation of Automated Vehicles, In: Proceedings IEEE Intelligent Vehicles Symposium, Changshu, Suzhou, China, 2018

MOST, T., J. WILL: Sensitivity analysis using the Metamodel of Optimal Prognosis., Proceedings Weimarer Optimization and Stochastic Days 8.0, Weimar, Germany, 2011

PÜTZ, A., ZLOCKI, A., BOCK, J., ECKSTEIN, L.: System validation of highly automated vehicles with a database of relevant traffic scenarios., 12th ITS European Congress, Strasbourg, France, 2017

RUBINSTEIN, R. Y.: Simulation and the Monte Carlo Method., New York: John Wiley & Sons, 1981

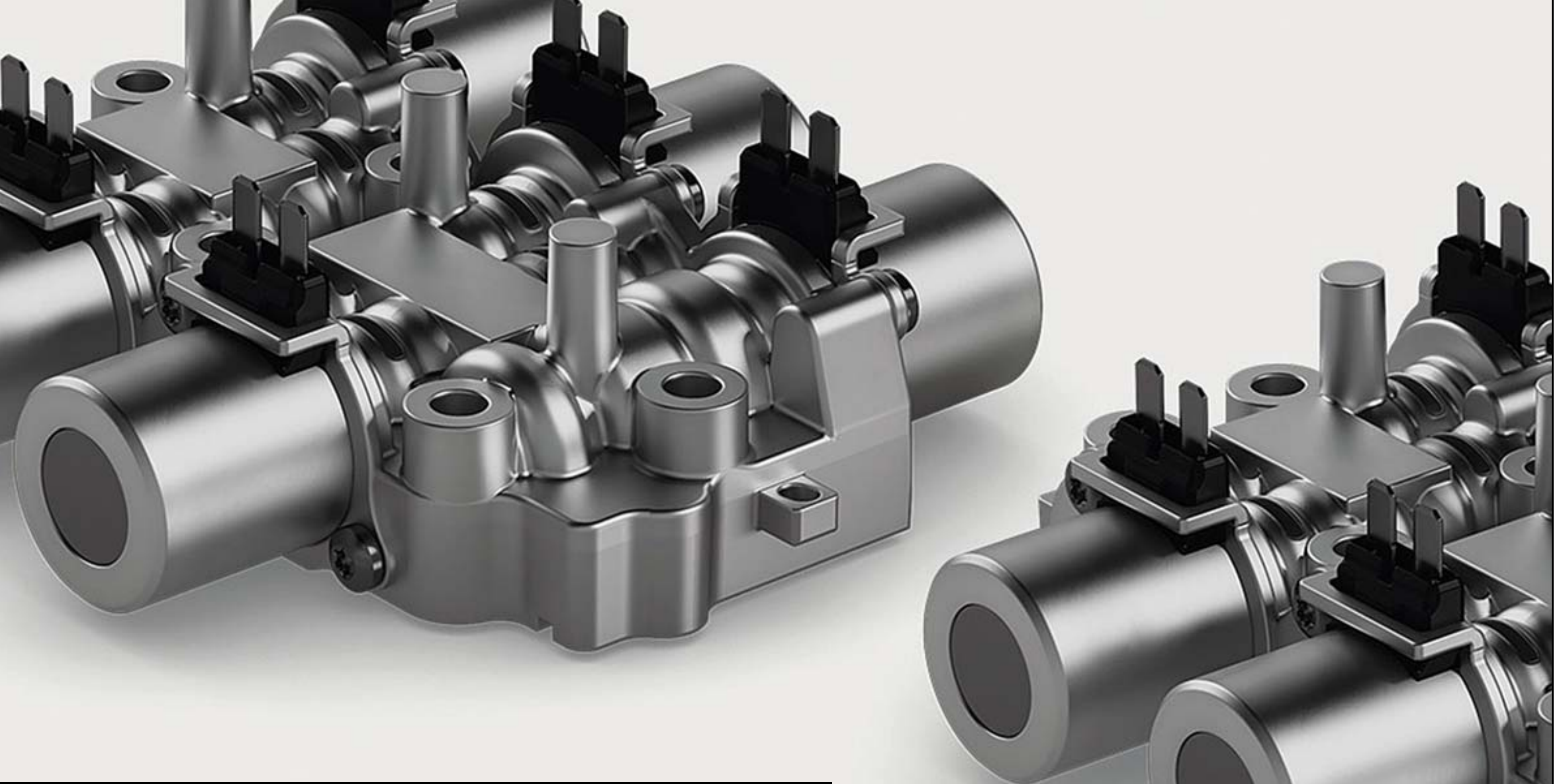

CUSTOMER STORY // AUTOMOTIVE ENGINEERING

OPTISLANG IN THE FUNCTIONAL DEVELOPMENT OF HYDRAULIC VALVES

optiSLang serves as a link between CFD and system simulations, as well as subsequent optimizations to derive geometric valve designs from customer requirements within the shortest possible time.

Simulation task and general procedure

Functionality of a 4/4-way valve

The product at the center of the optimization is a 4/4-way valve (FINDEISEN), which is used in mechatronics for the automatic gear shifting of a passenger car (see Figure 1). The aim of the hydraulic gearshift is to actuate or operate the gear adjuster via an electrical control signal (current). The gear adjuster is designed with a piston between two chambers. In order to move the piston, oil is pumped into a chamber (PA, PB), whereupon the pressure rises, a force is exerted on the piston and it then moves (gearshift). The opposite chamber must be emptied at the same time (BT, AT) so that no counterforce occurs. The oil flow is controlled via the directional control valve by opening or closing the control edges. By adjusting the flow areas, the flow rate varies according to the orifice equation (MATTHEIS, RENIUS) with

$$Q \sim A(X)\sqrt{dp} \qquad (1)$$

Q is the flow rate, A(X) the open area, dp the pressure difference and X the stroke. Since the area changes over the stroke, the flow rate can be adjusted as a function of the piston position. To adjust the stroke, a proportional solenoid is located on one side of the valve, which generates a force as a function of the current. A spring force acts as a counterforce ensuring an equilibrium of forces between spring and magnet in a defined position, depending on the magnetic force.

Description of the optimization task

Main objective of the investigation is the increase of the flow rate through the valve. In addition to the spring and magnetic forces, flow forces only act on the system during the flow. These forces generate directional disturbances in the dynamic behavior (Q-I characteristic curve) which must be kept as small as possible (FINDEISEN, HUGEL).

The flow forces are only a secondary precondition in this investigation. In common designs these are already optimized, however they must not be neglected, because otherwise already solved problems become visible again, e.g. the peaks in the A-branch move apart.

Figure 2 shows a Q-I curve, where the A-branch (left) realizes the PA or BT flow and the B-branch (right) generates the PB or AT flow. Thus four different flow areas are relevant for the optimization.

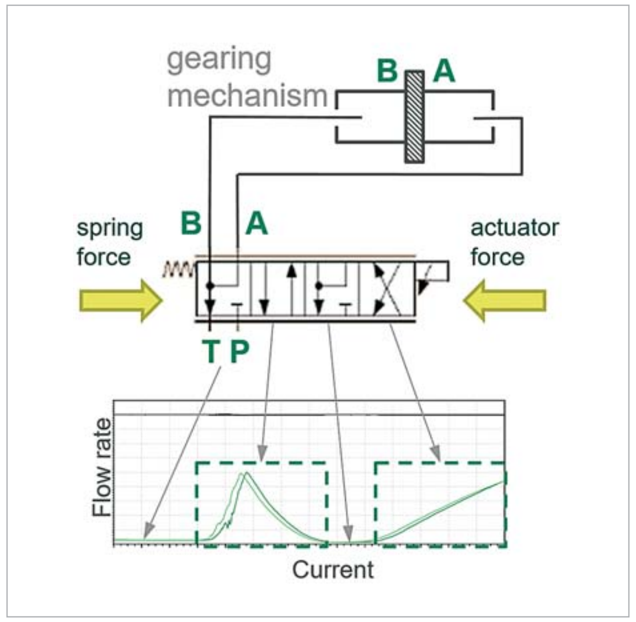

Fig. 1: Switching symbol and explanation of function including volumetric-flow / flow-characteristic curve (Q-I)

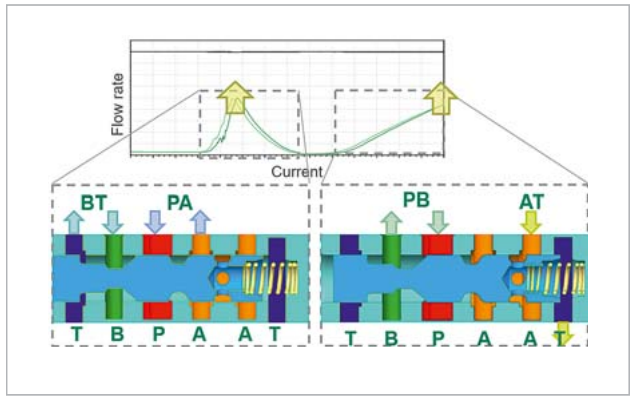

Fig. 2: Q-I characteristic curve with optimization target (yellow arrows) and valve geometry for the PA(BT) and PB(AT) switching positions

Simulation setup and execution

Potential analysis out of the system simulation

Since the optimization task has to be carried out under enormous time pressure, the focus must first be set correctly. In total there are four different port flows, each of which can be influenced by a variation of different geometric parameters. In order to get a feeling for the importance of the individual port flows (flow forces and flow rates) on the Q-I curve, a potential analysis is started. Therefrom the potential of a possible change is to be estimated , in order to carry out a detailed optimization of the geometric parameters only for the relevant control edges.

The system simulation model of the directional control valve is used as the basis for the potential analysis (see Figure 3). The system simulation model generates a Q-I(t) characteristic curve (time-dependent), whereby results from the CFD simulation are used as input. These CFD fields are scaled for the potential analysis.

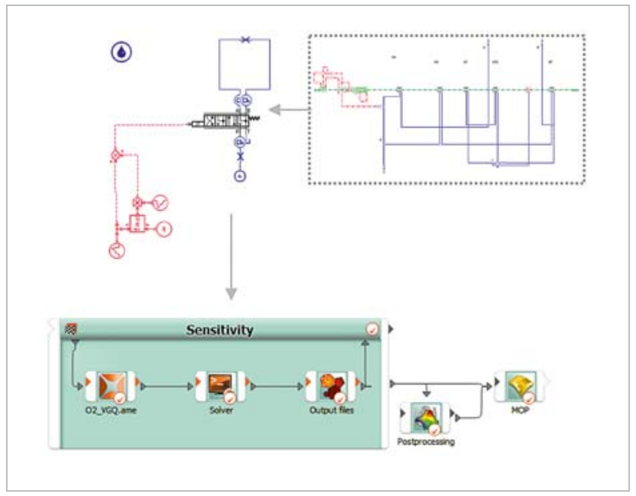

Fig. 3: System simulation model (AMESim, above) and integration into a sensitivity analysis in optiSLang (below)

In the sensitivity analysis, the scalars (and thus the fields) are varied stochastically in order to simulate the Q-I characteristic curve as a function of the field scaling. Although the scaling is not based on an actual geometry fit, it can be used to estimate the potential of each field fit.

Figure 4 shows the Q-I characteristic curve variation (signal plot) based on the field scaling factors and the COP matrix from optiSLang. The variation ranges of the scaling factors are the same, so that their importance can be read directly in the COP matrix.

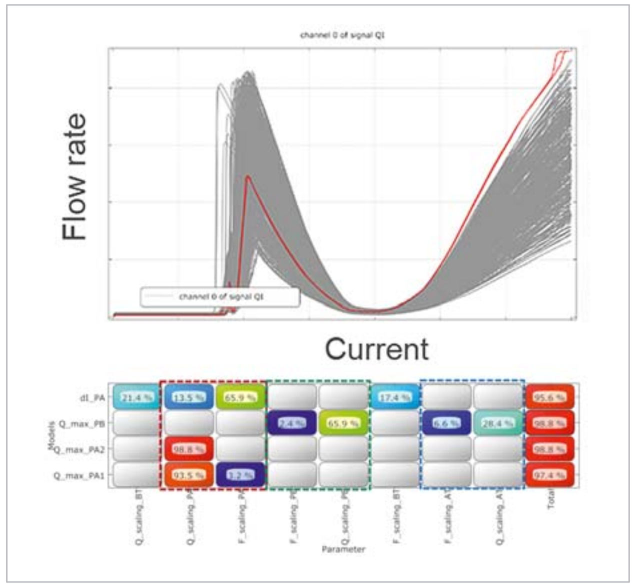

Fig. 4: Q-I characteristic curve variation (top) and COP matrix (bottom) for potential analysis

For the flow rates in the A branch (Q_max_PA1&2), it is shown that the flow rate of the PA flow has the greatest influence (red dotted). For the PB flow (Q_max_PB), the picture is somewhat different. Here both PB and AT must be optimized (green and blue dashed). An important parameter related to the flow forces is the peak offset dI_PA. In

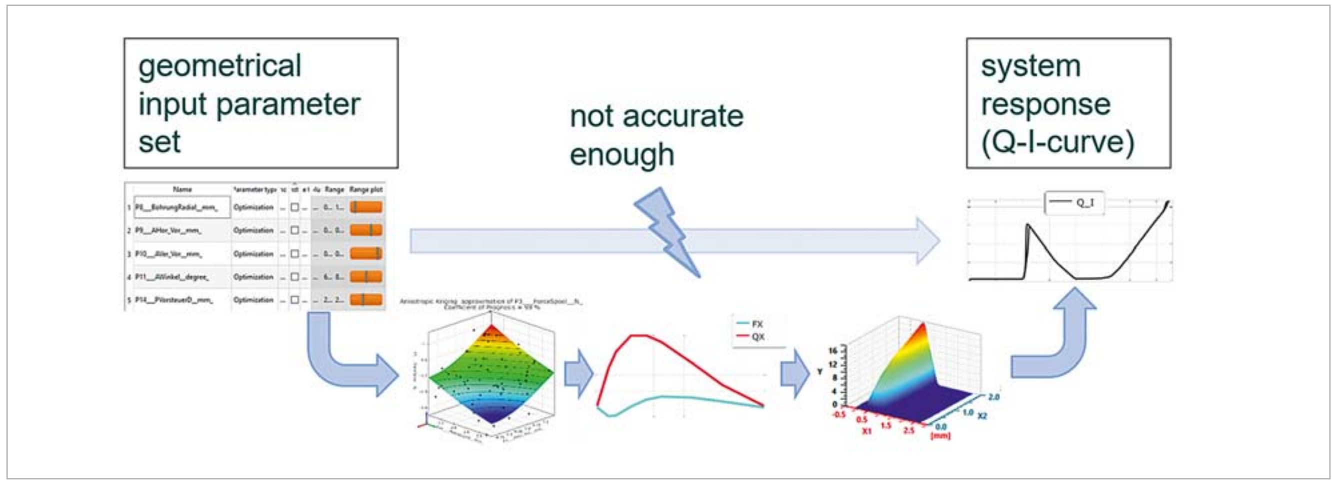

Fig. 5: Procedure for coupling between geometric quantities and system response

this case it can be seen that the flow forces PA and BT have an influence on it. These must always be taken into account in the subsequent optimization process.

Coupling between CFD and system simulation in optiSLang

The potential analysis shows which one of the flow fields has a large influence on the Q-I curve, but it does not show exactly what the geometry looks like that leads to this change.

Figure 5 shows a schematic diagram of the procedure. In principle, it is possible to integrate a variable-stroke opening surface directly into the system simulation with the aid of functions. However, as soon as flow forces play a major role, the models and approximation possibilities are not accurate enough. For this reason, another solution must be found.

This solution lies in the meta-modeling (MOP-solver, MOST, WILL) of the flow force in dependence of geometric parameters. For this purpose, a parametric CFD model (see chapter: MOP creation on the basis of CFD results) must be created in advance. Subsequently, a MOP is generated and integrated into optiSLang (MOP-solver). During the calculation, the MOP is interpolated, whereby a single MOP is available for each stroke position. A characteristic curve (force or flow rate over distance) is then generated and combined into a field using the analytical relationship from equation (1). This field can later be generated for the system simulation using the python script integrated in optiSLang. Since the system simulation is now able to simulate the Q-I characteristic curve, an optimization can be started on this basis for characteristic values, e.g. flow rate at the A port or peak offset.

MOP creation on the basis of CFD results

The heart of the Q-I characteristic curve optimization is the CFD-MOP (HUGEL). Since this is to be interpolated, the COP must be as good (i.e. close to 100%) as possible, which leads to a larger number of design points. At the same time, the CFD simulation should be robust, sufficiently precise and converged. Since all these requirements stand in conflict with the temporally strongly limited task, the workflow must be executed robustly, i.e. for each geometry which can be simulated a proper negative volume (flow rate) must be provided, a grid must be produced with regard to local refinements and a flow calculation must be computed up to convergence (see Figure 6).

The parameter variation (stochastically distributed input parameters, advanced Latin Hyper Cube and the subsequent MOP generation) is controlled by optiSLang and guarantees an optimal ratio between simulation time and quality of the metamodel.

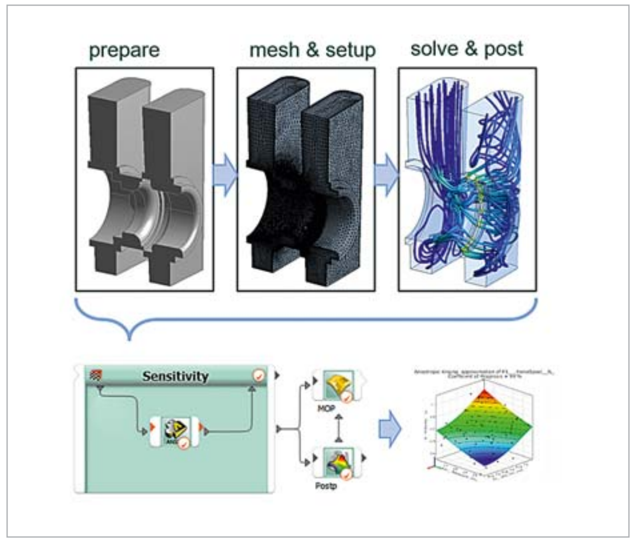

Fig. 6: Integration of ANSYS-Workbench (CFX) in optiSLang for MOP creation for the coupled system

With the help of the COP matrix the suitability of the MOP for interpolation can be investigated. The results show that these are larger than 97% and can therefore be used for further applications.

Optimization system

Since the MOPs of the CFD simulation are sufficiently accurate, the overall system can now be examined. Figure 7 shows the structure in optiSLang. The sensitivity system (left) generates a distribution of the geometric parameters, whereby the forces and flow rates are interpolated using the MOP (based on the CFD results). The data is then bundled in a calculator, processed onwards and forwarded to the python script. At this point the flow fields for the system simulation are created. Afterwards, a standard "AMESim in optiSLang" workflow is started.

Based on the results of the sensitivity analysis, a MOP is generated. Since the COPs are of high quality, the optimization may be started directly on the MOP (much faster). The re-evaluation system generated by optiSLang can subsequently be utilized to run a separate system simulation for the best design.

Various optimizations are started, whereby these only differ according to their criteria. For example, the subcriterion peak misalignment is constrained once barely and once very narrowly.

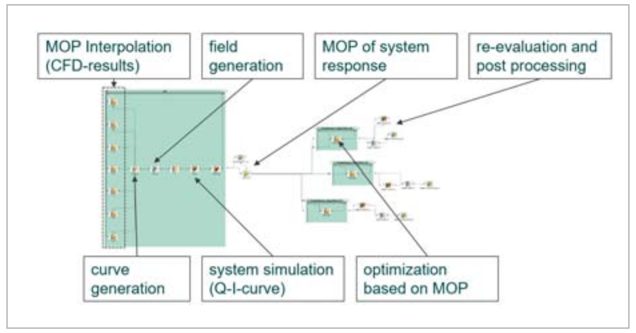

Fig. 7: Coupled Optimization System with subsequent MOP-based Optimization (3 x evolutionary algorithm with different criteria)

Results and re-evaluation

The coupled system delivers several results. First, the COP matrix of the sensitivity analysis is examined more precisely (see Figure 8). The geometric parameters are now displayed in dependency of the system results, which were evaluated on the Q-I characteristic curve. It is noticeable that the COPs are very large, meaning that the MOP is suitable for optimization. The relevant parameters (for the selected variation range) can also be read here (grey dashed).

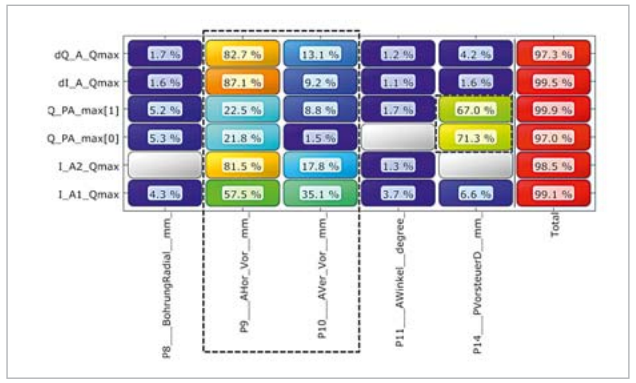

Fig. 8: COP matrix of the coupled system (sensitivity analysis)

Based on this MOP, an optimization by means of an evolutionary algorithm is started. It shows that the external goal to increase the flow rate can be realized without problems. On the basis of this knowledge, the flow rate is only defined as a constraint. The gradient of the characteristic curve and/or the peak offset are used as optimization targets.

The result of a multi-target optimization leads to a Pareto front (see Figure 9), which shows the best designs with regard to the target criteria. The re-evaluated designs, i.e. those recalculated in the system simulation, are shown in green. It becomes apparent that the Pareto front of the MOP optimization is smoother than that of the recalculated designs, but the differences are largely negligible.

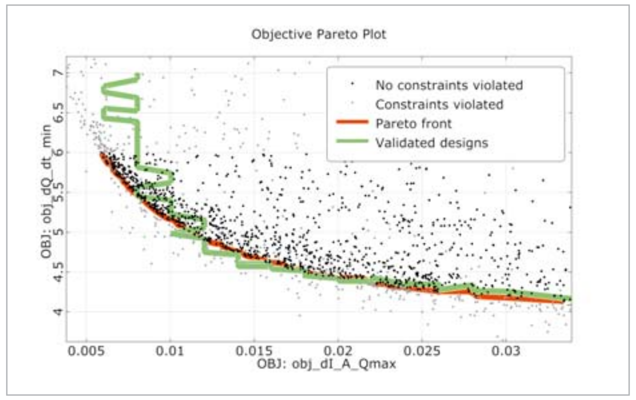

Fig. 9: Pareto front with validated design points

On the basis of the Pareto front, a compromise needs to be found between the two criteria. Therefore, the Q-I-characteristics are considered again. Using this as a basis, a set of parameters containing geometric parameters is derived. Therefrom a concrete design can be obtained.

However, it must be taken into account that the re-evaluated designs were also generated with the help of CFD-MOP. This results in the necessity of a second re-evaluation, i.e. a two-stage re-evaluation.

The process in Figure 6 is repeated with the parameters of the optimized design. Figure 10 (see next page) shows the flow rate and the flow force over the stroke for the MOP interpolated and recalculated variants. The shown convergence of both curves is very satisfactory. The high COP quality of the CFD-MOP can also be seen here.

Finally, the test result of the reference (green) and the target variant (purple) can be compared (see Figure 11). This shows that the gradient in the falling A-branch (optimization criterion) hardly varies, although the flow rate has increased significantly. The flow rates were also significantly increased.

Summary and outlook

When optimizing the 4/4-way valve, various partial ranges for Q-I characteristic curve optimization are possible. In order to analyze which of the ranges have the greatest influence, a potential analysis is performed. This shows the

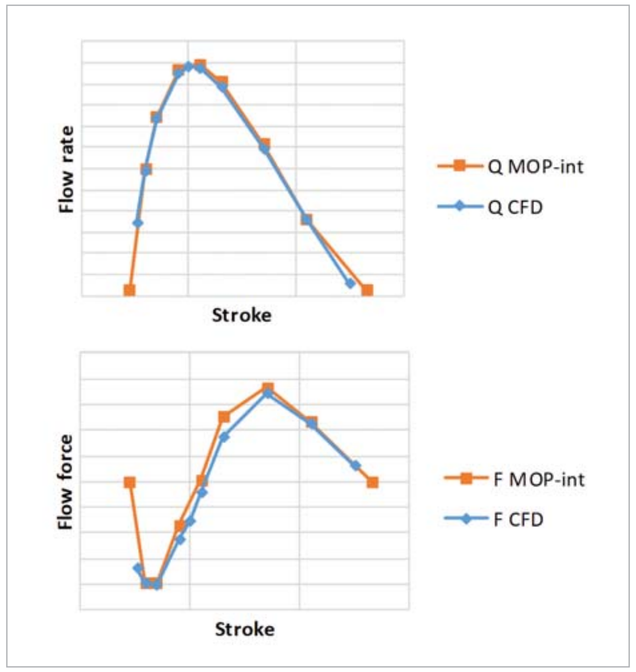

Fig. 10: Volume flow and flow force over the stroke for MOP interpolation and re-evaluated CFD simulation

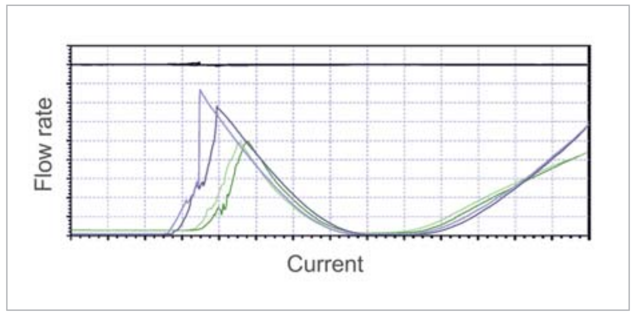

Fig. 11: Measurement results (Q-I characteristic) of the first prototypes (purple) compared to the reference (green)

large influence of the PA, PB and AT flows on the target parameters. By creating a MOP with optiSLang and CFX a correlation between flow forces, flow rates and geometric parameters can be identified. If this MOP is integrated into a coupled system simulation controlled by optiSLang, a relationship between transient behavior (Q-I characteristic) and geometric parameters can be calculated. This is used to calibrate the characteristic to the target functions. Using the workflow shown, a geometry that meets the optimization goals can be found and produced. In addition it offers to the customer the possibility to react quickly to the adaption of the target functions.

The next steps are a robustness analysis using production scatter and, if necessary, an adjustment of the tolerance width of the most important parameters with optiSLang.

Author //
Johannes Krebs (Hilite Germany GmbH)

References

www.dynardo.de: Change Log ANSYS optiSLang. URL https://www.dynardo.de/
FINDEISEN, D.; FINDEISEN, F.: Ölhydraulik – Handbuch für die hydrostatische Leistungsübertragung in der Fluidtechnik, 4 Auflage. Springer-Verlag Berlin Heidelberg 1994, S. 475-S. 563

MATTHEIS, H. J.; RENIUS, K., T.: Einführung in die Ölhydraulik, 4 Auflage, Teubner Verlag Stuttgart – Leipzig – Wiesbaden, 2003, S. 56.

MOST, T., WILL, J.: Metamodel of Optimal Prognosis – an automatic approach of variable reduction and optimal metamodel selection. In: Proceedings 5th WOST 2008, Weimar, Germany, 2008

HUGEL, C., SLEZIONA C., KREBS, J.: Optimierung einer Kolbengeometrie zur Strömungskraftkompensation in einem Druckregelventil, WOST 2016, Weimar, Germany, 2016

Contact & Distributors

Worldwide

Dynardo GmbH
Steubenstraße 25
99423 Weimar
Phone: +49 (0)3643 9008-30
Fax.: +49 (0)3643 9008-39
www.dynardo.de
contact@dynardo.de

Dynardo Austria GmbH
Office Vienna
Wagenseilgasse 14
1120 Vienna
www.dynardo.at
contact@dynardo.at

Dynardo US, Inc.
315 Montgomery Street
9th and 10th Floor
San Francisco, CA 94104
USA
www.dynardo.com
ralf.lampert@dynardo.com

Worldwide distribution of ANSYS optiSLang
ANSYS, Inc.
Canonsburg
www.ansys.com

Worldwide distribution of optiSLang
LightTrans GmbH
Jena
www.lighttrans.de

Germany
CADFEM GmbH
Grafing b. München
www.cadfem.de

Austria
CADFEM (Austria) GmbH
Vienna
www.cadfem.at

Switzerland
CADFEM (Suisse) AG
Aadorf
www.cadfem.ch

Czech Republic, Slovakia, Hungary
SVS FEM s.r.o.
Brno-Židenice
www.svsfem.cz

Sweden, Denmark, Finland, Norway
EDR & Medeso AB
Västerås
www.edrmedeso.com

United Kingdom of Great Britain and Northern Ireland
CADFEM UK CAE Ltd
Croydon, Surrey
www.cadfemukandireland.com

Ireland
CADFEM Ireland Ltd
Dublin
www.cadfemukandireland.com

Turkey
FIGES A.S.
Istanbul
www.figes.com.tr

North Africa
CADFEM Afrique du Nord s.a.r.l.
Sousse
www.cadfem-an.com

Russia
CADFEM CIS
Moscow
www.cadfem-cis.ru

India
CADFEM Engineering Services India
Hyderabad
www.cadfem.in

USA

CADFEM Americas, Inc.
Farmington Hills, MI
www.cadfem-americas.com

Ozen Engineering Inc.
Sunnyvale, CA
www.ozeninc.com

USA/Canada
SimuTech Group Inc.
Rochester, NY
www.simutechgroup.com

Japan
TECOSIM Japan Limited
Saitama
www.tecosim.co.jp

Korea
TaeSung S&E Inc.
Seoul
www.tsne.co.kr

China
PERA-CADFEM Consulting Inc.
Beijing
www.peraglobal.com

Publication details

Publisher
Dynardo GmbH
Steubenstraße 25
99423 Weimar
www.dynardo.de
contact@dynardo.de

Executive Editor & Layout
Henning Schwarz
henning.schwarz@dynardo.de

Registration
Local court Jena: HRB 111784

VAT Registration Number
DE 214626029

Publication
worldwide

© Images
metamorworks - stock.adobe.com: p. 27